Published for SISSA by Springer

Received: August 20, 2022
Revised: July 20, 2023
Accepted: October 3, 2023
Published: October 16, 2023

JHEP10(2023)091

A new approach to color-coherent parton evolution

Florian Herren,[a] **Stefan Höche,**[a] **Frank Krauss,**[b] **Daniel Reichelt**[b] **and Marek Schönherr**[b]

[a] *Fermi National Accelerator Laboratory, Kirk Rd & Pine St, Batavia, IL, 60510, U.S.A.*
[b] *Institute for Particle Physics Phenomenology, Durham University, Science Laboratories, South Rd, Durham DH1 3LE, U.K.*

E-mail: florian.s.herren@gmail.com, shoeche@fnal.gov, frank.krauss@durham.ac.uk, daniel.reichelt@durham.ac.uk, marek.schoenherr@durham.ac.uk

Abstract: We present a simple parton-shower model that replaces the explicit angular ordering of the coherent branching formalism with a differentially accurate simulation of soft-gluon radiation by means of a non-trivial dependence of the splitting functions on azimuthal angles. We introduce a global kinematics mapping and provide an analytic proof that it satisfies the criteria for next-to leading logarithmic accuracy. In the new algorithm, initial and final state evolution are treated on the same footing. We provide an implementation for final-state evolution in the numerical code Alaric and present a first comparison to experimental data.

Keywords: Parton Shower, Resummation

ArXiv ePrint: 2208.06057

Open Access, © The Authors.
Article funded by SCOAP[3].

https://doi.org/10.1007/JHEP10(2023)091

Contents

1 Introduction

Parton showers are a cornerstone of computer simulations for high-energy collider physics [1, 2]. They implement the evolution of QCD from the hard scales to be probed by experiments, to the low scale of hadronization, where the transition of quasi-free partons (the quarks and gluons of perturbative QCD) to observable hadrons occurs. In this process, a number of additional partons are generated according to evolution equations that are based on the factorization properties of QCD amplitudes in the soft and collinear limits. The most

JHEP10(2023)091

commonly used parton showers can be thought of as numerical implementations of the DGLAP equations [3–6], but various other approaches exist [7–9].

The first generation of parton shower programs [10–14] was developed four decades ago. Implementations differed in the way in which the ordering inherent to the evolution equations was realized in the simulation, and how the kinematics of the emissions were set up. Color coherence, manifesting itself through angular ordering [15–20] became a guiding principle for the construction of parton showers [21, 22]. Some of these parton showers were also improved using spin correlation algorithms [23–26]. Increasing precision requirements, especially in preparation for the Large Hadron Collider (LHC), mandated more precise Monte-Carlo simulations. The matching of parton showers to next-to-leading order calculations [27–33] and the merging of calculations for varying jet multiplicity [34–44] became focus points of event generator development. The correspondence between fixed-order infrared subtraction schemes and parton showers was identified as central to a correct matching procedure, leading to the construction of algorithms with a dipole-local momentum mapping and ordering in transverse momentum [45–52].

These newly developed algorithms were found to have significant drawbacks in terms of their logarithmic accuracy [53]. The resummation of observables at leading logarithmic (LL) accuracy is relatively straightforward to achieve using a parton-shower algorithm. The resummation at next-to-leading logarithmic (NLL) precision however poses a number of challenges. The first generic technique to quantify the logarithmic accuracy of parton showers was presented in [53, 54] and consists of a set of fixed-order and all-order criteria, which can broadly be classified as tests related to kinematic recoil effects, and tests of color coherence. In the present manuscript, we will discuss only kinematic effects. A discussion of sub-leading color effects can be found for example in [55–67]. One of the main results of [53] was that the kinematics mapping in the transition from an n-particle to an $n+1$-particle final state should not alter the existing momentum configuration in a way that distorts the effects of the pre-existing emissions on observables. This criterion is formulated such that only the effects relevant at NLL precision can be extracted, by taking the limit $\alpha_s \to 0$ at fixed $\lambda = \alpha_s \ln v$, where v is the observable to be resummed. The algorithms in [47, 50, 52] do not satisfy the criteria for NLL precision, because their momentum mappings can generate recoil whose effect on existing emissions at commensurate scales does not vanish in the $\alpha_s \to 0$ limit. It is important to note that these failures to agree with known NLL resummation are not related to the effects of momentum and probability conservation discussed in [68]. In order to remedy the problem with NLL accuracy, new kinematics mapping schemes were developed in [54, 69–71]. The main difference of the new dipole schemes in [54, 71] compared to existing algorithms is that recoil is assigned according to the rapidity of the emission in the frame of the hard process, rather than the dipole frame, and that initial-state radiation is treated such that the interpretation of the hard system is unchanged for subsequent emissions.

We will approach the same problem from a different perspective. Recalling that color–coherent parton evolution is a consequence of the angular dependence of the soft eikonal, we will reformulate the radiator functions of [21] using a partial fractioning approach similar to the identified particle subtraction scheme in [72]. In addition, we note that in dipole

JHEP10(2023)091

and antenna showers the anti-collinear direction is inextricably linked to the direction of the color spectator. By lifting this restriction, we are able to construct an algorithm which allows the entire QCD multipole to absorb the recoil from parton branching, independent of the number of pre-existing emissions, and independent of their kinematics. The price for such a generic scheme is a dependence of the parton shower splitting functions on the azimuthal angle between the decay plane and the plane defined by the emitting parton and its color spectator. Our new formulation presents a major extension of existing parton shower formalisms in this regard, and it introduces the most generic form of a spin-averaged splitting function in four dimensions, with a dependence on all three phase-space variables of the radiated parton. Based on previous analyses [73, 74], it seems plausible that this scheme will considerably simplify the inclusion of higher-order corrections to the splitting kernels. We provide a first implementation of the new algorithm in the numerical code Alaric,[1] which will be made available as part of the event generator Sherpa [75–77].

This manuscript is organized as follows: In section 2 we revisit the soft singularity structure of QCD amplitudes and introduce our new decomposition of the soft eikonal. In section 3 we discuss the novel phase-space mapping and the corresponding phase-space factorization. In section 4 we detail how soft and collinear emissions are generated in a probabilistic picture. Section 5 is dedicated to the analytic proof of logarithmic accuracy, and the numerical validation in the $\alpha_s \to 0$ limit. Section 6 presents first numerical results for the process $e^+e^- \to$ hadrons, and section 7 contains an outlook.

2 The matching of soft to collinear radiators

We start the discussion by recalling the singularity structure of n-parton QCD amplitudes in the infrared limits.

If two partons, i and j, become collinear, the squared amplitude factorizes as

$$
\begin{aligned}
&{}_n\langle 1,\dots,n|1,\dots,n\rangle_n \\
&= \sum_{\lambda,\lambda'=\pm} {}_{n-1}\Big\langle 1,\dots,\not{i}(ij),\dots,\not{j},\dots,n\Big|\frac{8\pi\alpha_s}{2p_ip_j}P^{\lambda\lambda'}_{(ij)i}(z)\Big|1,\dots,\not{i}(ij),\dots,\not{j},\dots,n\Big\rangle_{n-1}\,,
\end{aligned}
\tag{2.1}
$$

where the notation $\not{i}$ indicates that parton i is removed from the original amplitude, and where (ij) is the progenitor of partons i and j. The functions $P^{\lambda\lambda'}_{ab}(z)$ are the spin-dependent DGLAP splitting functions. They depend on the momentum fraction z of parton i with respect to the mother parton, (ij), and on the helicities λ [3–6]. In the collinear limit, the momentum fraction is equal to an energy or light-cone momentum fraction. In this manuscript we will consider only spin-averaged splitting functions; algorithms for spin-dependent evolution are discussed in [23–26, 78].

In the limit that gluon j becomes soft, the squared amplitude factorizes as [79]

$$
{}_n\langle 1,\dots,n|1,\dots,n\rangle_n = -8\pi\alpha_s \sum_{i,k\neq j} {}_{n-1}\langle 1,\dots,\not{j},\dots,n|\mathbf{T}_i\mathbf{T}_k\, w_{ik,j}|1,\dots,\not{j},\dots,n\rangle_{n-1}\,,
\tag{2.2}
$$

[1] Alaric is an acronym for A Logarithmically Accurate Resummation In C++.

JHEP10(2023)091

where $\mathbf{T}_i$ and $\mathbf{T}_k$ are the color insertion operators defined in [72]. In the remainder of this section we will discuss the case of massless radiators only and focus on the eikonal factor, $w_{ik,j}$, and how it can be rewritten in a suitable form to match the spin-averaged splitting functions $P_{ab}(z)$ in the soft-collinear limit. Since our analysis concerns only the denominator of $w_{ik,j}$, it will apply to spin-correlated evolution as well. The eikonal factor is given by

$$w_{ik,j} = \frac{p_i p_k}{(p_i p_j)(p_j p_k)}\,, \tag{2.3}$$

and it can be written in terms of (frame-dependent) energies and angles as

$$w_{ik,j} = \frac{W_{ik,j}}{E_j^2}\,, \qquad \text{where} \qquad W_{ik,j} = \frac{1-\cos\theta_{ik}}{(1-\cos\theta_{ij})(1-\cos\theta_{jk})}\,. \tag{2.4}$$

We note that eq. (2.4) is symmetric in i and k, and that it encapsulates the complete soft singularity structure of the hard matrix element [79]. If we were to implement eq. (2.4) for each of the radiators i and k in the collinear limit, we would therefore double-count the most singular component of the emission probability [80]. This is known as the soft double-counting problem, which can be solved by following the technique of [21]. In this approach, $W_{ik,j}$ is written as a sum of two terms, which are enhanced only in either the ij- or kj-collinear limit:

$$\begin{aligned} &W_{ik,j} = \tilde{W}^i_{ik,j} + \tilde{W}^k_{ki,j}\,, \\ \text{where} \qquad &\tilde{W}^i_{ik,j} = \frac{1}{2}\left(\frac{1-\cos\theta_{ik}}{(1-\cos\theta_{ij})(1-\cos\theta_{jk})} + \frac{1}{1-\cos\theta_{ij}} - \frac{1}{1-\cos\theta_{jk}}\right). \end{aligned} \tag{2.5}$$

It is customary to define the z-axis to be aligned with the momentum p_i, such that we can write $\cos\theta_{jk}$ in terms of polar angles, θ^i_j, θ^i_k with respect to the axis defined by p_i, and the azimuthal angle ϕ^i_{jk} in the same frame. Note in particular that $\theta^i_l = \theta_{li}$, for any l.

$$\cos\theta_{jk} = \cos\theta^i_j \cos\theta^i_k + \sin\theta^i_j \sin\theta^i_k \cos\phi^i_{jk}\,. \tag{2.6}$$

When performing the azimuthal averaging, we find the simple result [21]

$$\frac{1}{2\pi}\int_0^{2\pi} \mathrm{d}\phi^i_{jk} \tilde{W}^i_{ik,j} = \frac{\tilde{I}^i_{ik,j}}{1-\cos\theta^i_j}\,, \qquad \text{where} \qquad \tilde{I}^i_{ik,j} = \begin{cases} 1 & \text{if} \quad \theta^i_j < \theta^i_k \\ 0 & \text{else} \end{cases}\,. \tag{2.7}$$

The behavior of $\tilde{I}^i_{ik,j}$ as a function of the polar angles is known as angular ordering, which means that the total probability for soft radiation averages to zero outside of a cone defined by the cusp angle θ^i_k of the radiating color dipole. This is the origin of the coherent branching formalism and the basis for angular ordered parton showers. It is instructive to investigate this radiation pattern in more detail. Figures 1(a) and 1(b) display the positive and negative contribution to the azimuthal integral, normalized to 2π, as a function of the polar angles. The partial radiator function $\tilde{W}^i_{ik,j}$ has a root at

$$\cos\phi^{i(0)}_{jk} = -\sqrt{\frac{1+\cos\theta^i_j}{1-\cos\theta^i_j}\,\frac{1-\cos\theta^i_k}{1+\cos\theta^i_k}} \tag{2.8}$$

JHEP10(2023)091

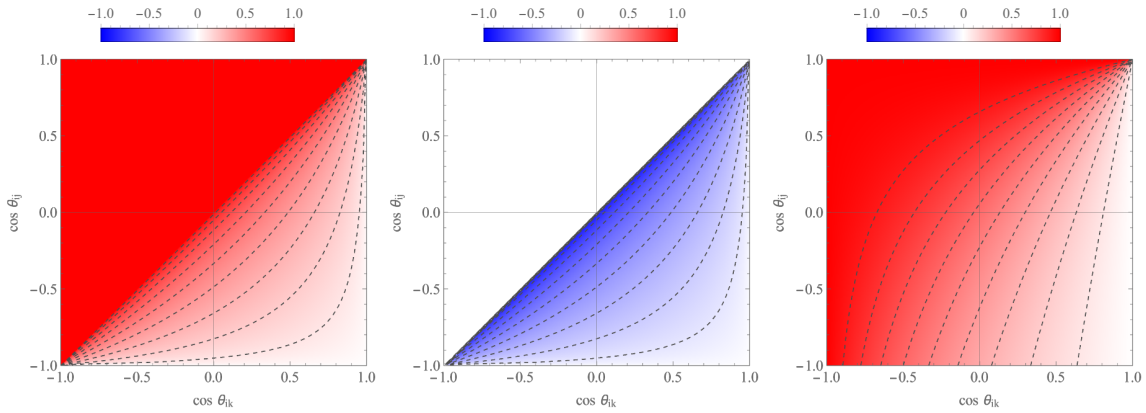

Figure 1. Azimuthally integrated radiator functions. Figures (a) and (b) show the positive and negative contributions to $\tilde{I}^i_{ik,j}$ arising from the additive matching in eq. (2.5), figure (c) displays $\bar{I}^i_{ik,j}$ from the multiplicative matching in eq. (2.9).

which falls inside the integration domain if $\theta^i_j > \theta^i_k$. In this case, the negative contribution to the azimuthal integral is equal in magnitude to the positive contribution, such that the average radiation probability vanishes identically. However, there is a strong modulation of this probability as a function of the azimuthal angle. If this modulation is not included in a parton-shower simulation, wide-angle soft radiation effects will only be captured correctly for observables that are sufficiently insensitive to the precise distribution of radiation in phase space.

A naive attempt to solving this problem would be to include the full azimuthal dependence of the radiator function in the Monte-Carlo simulation. Such an approach is bound to fail, because in the region $\theta^i_j > \theta^i_k$ one would need to sample the same amount of negative and positive weighted Monte-Carlo events, leading to an efficiency of exactly zero. We therefore adopt a different strategy, pioneered in [72], where the radiator function is partial fractioned such that it maintains strict positivity

$$W_{ik,j} = \bar{W}^i_{ik,j} + \bar{W}^k_{ki,j}\,, \qquad \text{where} \qquad \bar{W}^i_{ik,j} = \frac{1-\cos\theta_{ik}}{(1-\cos\theta_{ij})(2-\cos\theta_{ij}-\cos\theta_{jk})}\,. \tag{2.9}$$

Azimuthal averaging again leads to eq. (2.7), except that $\tilde{I}^i_{ik,j}$ is replaced by

$$\bar{I}^i_{ik,j} = \frac{1}{\sqrt{(\bar{A}^i_{ij,k})^2 - (\bar{B}^i_{ij,k})^2}}\,, \tag{2.10}$$

where

$$\bar{A}^i_{ij,k} = \frac{2-\cos\theta^i_j(1+\cos\theta^i_k)}{1-\cos\theta^i_k} \qquad \text{and} \qquad \bar{B}^i_{ij,k} = \frac{\sqrt{(1-\cos^2\theta^i_j)(1-\cos^2\theta^i_k)}}{1-\cos\theta^i_k}\,. \tag{2.11}$$

This function is shown in figure 1(c). As required, it approaches unity in the limit $\theta^i_j \to 0$, independent of the value of θ^i_k, and also for the special case of a back-to-back configuration,

JHEP10(2023)091

$\theta_k^i \to \pi$. While the Monte-Carlo efficiency of an algorithm using this technology will be reduced compared to plain angular ordered evolution, the obvious benefit is that eq. (2.9) allows to capture all angular correlations associated with the spin-summed soft eikonal, eq. (2.4). In contrast, traditional angular ordered evolution, which is based on eq. (2.7), does not populate the complete emission phase space, necessitating intricate matrix-element corrections and creating complications in higher-order matching [27]. We note again that the energy E_j in eq. (2.4) is frame dependent. This effect will be discussed in more detail in section 4.1.

In the limit where partons i and j are collinear, we can write the eikonal factor in eq. (2.3) as

$$w_{ik,j} \xrightarrow{i||j} w_{ik,j}^{(\text{coll})}(z) = \frac{1}{2p_i p_j} \frac{2z}{1-z}, \qquad \text{where} \qquad z \xrightarrow{i||j} \frac{E_i}{E_i + E_j}. \tag{2.12}$$

This can be identified with the leading term (in $1-z$) of the DGLAP splitting functions $P_{aa}(z)$, where[2]

$$\begin{aligned} P_{qq}(z) &= C_F \left(\frac{2z}{1-z} + (1-z) \right), \\ P_{gg}(z) &= C_A \left(\frac{2z}{1-z} + z(1-z) \right), \\ P_{gq}(z) &= T_R \left(1 - 2z(1-z) \right). \end{aligned} \tag{2.13}$$

To match the soft to the collinear splitting functions, we therefore replace

$$\frac{1}{2p_i p_j} P_{(ij)i}(z) \to \frac{1}{2p_i p_j} P_{(ij)i}(z) + \delta_{(ij)i}\, \mathbf{T}_i^2 \left[\frac{\bar{W}_{ik,j}^i}{E_j^2} - w_{ik,j}^{(\text{coll})}(z) \right], \tag{2.14}$$

where the two contributions to the gluon splitting function are treated as two different radiators [50]. This substitution introduces a dependence on a color spectator, k, whose momentum defines a direction independent of the direction of the collinear splitting. In general, this implies that splitting functions which were formerly dependent only on a momentum fraction along this direction, now acquire a dependence on the remaining two phase-space variables of the new parton. This is the most general form of a splitting kernel for spin-averaged parton evolution, which we will use in the following. In particular, the dependence on the azimuthal angle allows to define the recoil momentum such that NLL precision is maintained for any hard process, as discussed in more detail in section 5.

3 Momentum mapping and phase-space factorization

The mapping of Born momenta to a kinematic configuration after emission of additional partons is a key component of any parton shower algorithm. It is closely tied to the factorization of the Lorentz-invariant differential phase space element for a multi-parton configuration. Suitable momentum mappings will preserve the key features of previously

[2]Note that in contrast to standard DGLAP notation, we separate the gluon splitting function into two parts, associated with the soft singularities at $z \to 0$ and $z \to 1$.

JHEP10(2023)091

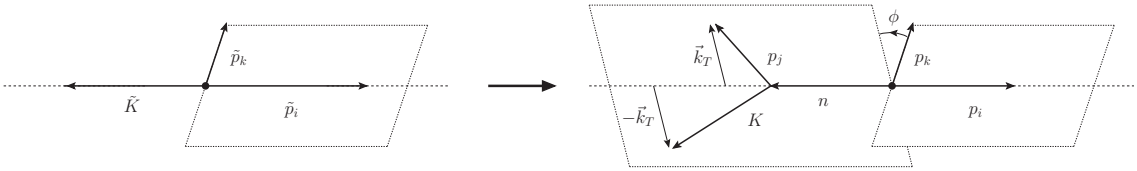

Figure 2. Sketch of the momentum mapping for final-state evolution. See the main text for details. Note that p_k does not participate in the shift, eq. (3.3), and only acts as a reference for the azimuthal angle ϕ.

simulated radiation, while an unsuitable mapping could skew the QCD radiation pattern up to a point where it becomes not only theoretically incorrect, but the differences become visible experimentally. A prime, although academic, example for the latter problem is a collinear unsafe mapping algorithm, in which the parton shower does not reflect the features of the collinear limit of the QCD matrix elements, eq. (2.3) and therefore introduces an error at leading logarithmic accuracy. A key requirement for the construction of any momentum mapping therefore is collinear safety, and all known parton-shower algorithms satisfy this constraint. An example for a problem which may only be seen in dedicated measurements was identified in [53]. It originates in a modification of existing soft momenta in subsequent emissions, that introduces an error in the simulated QCD radiation pattern at next-to-leading logarithmic accuracy. In the following, we will construct a generic, collinear and NLL safe momentum mapping for both final-state and initial-state radiation, which is inspired by the identified–particle dipole subtraction algorithm in [72]. We will provide the analytic proof of NLL safety in section 5.1 and sketch the additional steps that are required to match the parton shower to NLO calculations in appendix C.

We begin by describing the logic underpinning our new kinematics mapping, $\{\tilde{p}_l\} \to \{p_l\}$. We identify the splitter momentum, $\tilde{p}_i$, and define a recoil momentum, $\tilde{K}$, as the negative sum of all momenta in the radiating QCD multipole, *including* the momentum of the splitter (see also appendix A).[3] Together, the momenta $\tilde{K}$ and $\tilde{p}_i$ define the reference frame of the splitting, as shown schematically in figure 2 (left). The momentum of the color spectator, $\tilde{p}_k$, defines an additional direction, which provides the reference for the azimuthal angle, ϕ. In the first step of the mapping, the emitter momentum is scaled by a factor z, and the emitted momentum, p_j, is constructed with transverse momentum component $\vec{k}_T$ and suitable light-cone momenta. The color spectator remains unchanged, $p_k = \tilde{p}_k$. The recoil is absorbed by the overall multipole, such that after the emission we have $K \neq \tilde{K}$, while $K^2 = \tilde{K}^2$. In particular, the multipole after the emission acquires a transverse momentum with respect to $\tilde{K}$. This is shown schematically in figure 2 (right). To compensate for both the transverse and the longitudinal recoil, the overall multipole is boosted to its original frame of reference. This changes all momenta and effectively distributes the recoil among them, generating changes of the order of $\mathrm{k}_T/\sqrt{K^2}$, which vanish in the infrared limits. We will make use of this fact in section 5.1.

[3] This construction differs from the traditional choice in parton and dipole showers, where the splitter and recoil partner are disjoint.

JHEP10(2023)091

A collinear safe momentum mapping requires that for any two massless collinear partons, i and j, the momenta behave as

$$p_i \xrightarrow{i\|j} z\,\tilde{p}_i\,, \qquad p_j \xrightarrow{i\|j} (1-z)\,\tilde{p}_i\,. \tag{3.1}$$

In the exact limit, $\cos\theta_{ij} = 0$, the splitting variable z is uniquely defined and given by

$$z = \frac{p_i n}{(p_i + p_j)n}\,, \tag{3.2}$$

where n is an arbitrary auxiliary vector that satisfies $\tilde{p}_i n \neq 0$. Note that n can be either light-like, time-like or space-like, as long as $\tilde{p}_i n \neq 0$. In order to construct a collinear-safe momentum mapping for arbitrary values of the two-particle virtuality $p_i p_j$, we can simply use the first part of eq. (3.1) away from this limit. This implies in particular that p_i retains its direction, and that all angular radiator functions involving p_i remain unchanged.

A second important constraint for the mapping is overall four-momentum conservation. We satisfy this by defining a vector $\tilde{K}$ to be a combination of the momenta $\{\tilde{p}_1, \ldots, \tilde{p}_{j-1}, \tilde{p}_{j+1}, \ldots, \tilde{p}_n\}$, and by using the shift

$$p_i = z\,\tilde{p}_i\,, \qquad n = \tilde{K} + (1-z)\,\tilde{p}_i\,, \tag{3.3}$$

which implies $p_i + n = \tilde{p}_i + \tilde{K}$. The remaining task is to construct two new vectors, K and p_j, such that $K^2 = \tilde{K}^2$, and such that p_j satisfies the collinear safety constraint, eq. (3.1). The momenta in $\tilde{K}$ are mapped to new momenta by a Lorentz transformation that is defined in terms of $\tilde{K}$ and K. The simplest way to obtain the new momenta is by means of a light-cone parametrization [81]. With the help of the light-like vector

$$\bar{n} = n - \frac{n^2}{2\tilde{p}_i n}\,\tilde{p}_i = \tilde{K} - \kappa\,\tilde{p}_i\,, \qquad \text{where} \qquad \kappa = \frac{\tilde{K}^2}{2\tilde{p}_i\tilde{K}}\,, \tag{3.4}$$

we can write

$$\begin{aligned} p_j &= v\,\bar{n} + \frac{1}{v}\frac{\mathrm{k}_\perp^2}{2\tilde{p}_i\tilde{K}}\,\tilde{p}_i - k_\perp\,, \qquad \text{where} \qquad v = \frac{p_i p_j}{p_i\tilde{K}} \\ K &= (1-v)\,\bar{n} + \frac{1}{1-v}\frac{\mathrm{k}_\perp^2 + \tilde{K}^2}{2\tilde{p}_i\tilde{K}}\,\tilde{p}_i + k_\perp\,. \end{aligned} \tag{3.5}$$

Equation (3.5) makes it manifest that $\tilde{K}$ absorbs the newly generated transverse and anti-collinear momentum when parton (ij) is put off-shell, such that overall momentum conservation is satisfied. This leads to the identity[4]

$$\mathrm{k}_\perp^2 = v(1-v)\,2p_jK - v^2K^2 = v(1-v)(1-z)\,2\tilde{p}_i\tilde{K} - v^2\tilde{K}^2\,. \tag{3.6}$$

Note that $\mathrm{k}_\perp^2$ is proportional to v and therefore tends to zero in the collinear limit $\cos\theta_j^i \to 0$. Inserting this relation into eq. (3.5) makes both collinear safety and overall four-momentum conservation of the kinematics mapping manifest.

$$\begin{aligned} p_j &= (1-z)\,\tilde{p}_i + v\big(\tilde{K} - (1-z+2\kappa)\,\tilde{p}_i\big) + k_\perp\,, \\ K &= \qquad \tilde{K} - v\big(\tilde{K} - (1-z+2\kappa)\,\tilde{p}_i\big) - k_\perp\,. \end{aligned} \tag{3.7}$$

[4] In eq. (3.6), the variable v takes the place of the splitting variable z in a standard collinear parametrization.

JHEP10(2023)091

In order to determine a reference direction for the azimuthal angle $\phi = \arctan(\mathrm{k}_y/\mathrm{k}_x)$, we note that the soft radiation pattern of eq. (2.9) must be correctly generated. To achieve this we decompose the transverse momentum as

$$k_\perp^\mu = \mathrm{k}_\perp \left(\cos\phi \, \frac{n_\perp^\mu}{|n_\perp|} + \sin\phi \, \frac{l_\perp^\mu}{|l_\perp|} \right) , \tag{3.8}$$

where the reference axes $n_\perp$ and $l_\perp$ are given by the transverse projections[5]

$$n_\perp^\mu = p_k^\mu - \frac{p_k \bar{n}}{\tilde{p}_i \tilde{K}} \, \tilde{p}_i^\mu - \frac{p_k \tilde{p}_i}{\tilde{p}_i \tilde{K}} \, \bar{n}^\mu , \qquad \text{and} \qquad l_\perp^\mu = \varepsilon^\mu{}_{\nu\rho\sigma} \, \tilde{p}_i^\nu \, \bar{n}^\rho \, n_\perp^\sigma . \tag{3.9}$$

Because the differential emission phase-space element, eq. (3.14), is a Lorentz-invariant quantity, the azimuthal angle ϕ is Lorentz invariant. It can be expressed as

$$\phi = \arccos \frac{(p_i p_j)(p_k \bar{n}) + (p_i p_k)(p_j \bar{n}) - (p_i \bar{n})(p_j p_k)}{\sqrt{2(p_i p_j)(p_j \bar{n})} \sqrt{2(p_i p_k)(p_k \bar{n})}} . \tag{3.10}$$

This allows us to write the emission phase space in a frame-independent way. After the momenta p_i, p_j and K are constructed, the momenta $\{p_l\}$ used to define $\tilde{K}$ are subjected to a Lorentz transformation, which can be written as [72]

$$p_l^\mu \to \Lambda_\nu^\mu(\tilde{K}, K) \, p_l^\nu , \qquad \text{where} \qquad \Lambda_\nu^\mu(\tilde{K}, K) = g_\nu^\mu - \frac{2(K+\tilde{K})^\mu (K+\tilde{K})_\nu}{(K+\tilde{K})^2} + \frac{2K^\mu \tilde{K}_\nu}{\tilde{K}^2} . \tag{3.11}$$

If needed, the event is restored to the lab frame, as described in appendix A. We list the precise algorithm for the construction of final-state splittings in section A.1, and give the algorithm for the construction of initial-state splittings in section A.2. The initial-state kinematics are obtained by the simple replacement $z \to x = 1/z$, as indicated by crossing relations.

The last remaining task is to determine the differential emission phase space element. We will outline how to do this for pure final-state evolution, where the recoil partner $\tilde{K}$ corresponds to the sum of the initial state momenta. This covers the important case of the decay of a color-neutral, massive particle, such as a Z-boson at LEP. Since K, $\tilde{K}$ and n are treated as outgoing, they appear with negative energy component, which requires the explicit compensation of a number of minus signs that do not appear in the case where $\tilde{K}$ corresponds to a part of the final state. The general discussion can be found in appendix B.

The differential phase-space element for $(n-1)$ hard momenta, $\{p_1, \ldots, p_{j-1}, p_{j+1}, \ldots, p_n\}$, and one soft momentum, p_j, is defined as

$$\mathrm{d}\Phi_n(p_a, p_b; p_1, \ldots, p_n) = \left[\prod_{i=1}^{n} \frac{1}{(2\pi)^3} \frac{\mathrm{d}^3 p_i}{2p_i^0} \right] (2\pi)^4 \delta^{(4)} \left(p_a + p_b - \sum p_i \right) . \tag{3.12}$$

[5] In kinematical configurations where p_k^μ is a linear combination of p_i^μ and $\bar{n}^\mu$, $n_\perp$ in the definition of eq. (3.8) vanishes. It can then be computed using $n_\perp = \varepsilon^{\mu j}{}_{\nu\rho} \, p_i^\nu \, \bar{n}^\rho$, where $j \in \{1, 2, 3\}$ may be any index that yields a nonzero result. Note that in this case the matrix element cannot depend on the azimuthal angle.

JHEP10(2023)091

It can be written in terms of the differential phase-space element for the momenta $\{\tilde{p}_1, \ldots, \tilde{p}_{j-1}, \tilde{p}_{j+1}, \ldots, \tilde{p}_n\}$ before the mapping

$$\mathrm{d}\Phi_{n-1}(\tilde{p}_a, \tilde{p}_b; \tilde{p}_1, \ldots, \tilde{p}_{j-1}, \tilde{p}_{j+1}, \ldots, \tilde{p}_n) = \left[\prod_{\substack{i=1 \\ i\neq j}}^{n} \frac{1}{(2\pi)^3} \frac{\mathrm{d}^3\tilde{p}_i}{2\tilde{p}_i^0}\right] (2\pi)^4 \delta^{(4)}\left(\tilde{p}_a + \tilde{p}_b - \sum_{i\neq j} \tilde{p}_i\right), \tag{3.13}$$

and the ratio of differential phase-space elements after and before the mapping

$$\mathrm{d}\Phi_{+1}(\tilde{p}_a, \tilde{p}_b; \tilde{p}_1, \ldots, \tilde{p}_{j-1}, \tilde{p}_{j+1}, \ldots, \tilde{p}_n; p_j) = \frac{\mathrm{d}\Phi_n(p_a, p_b; p_1, \ldots, p_n)}{\mathrm{d}\Phi_{n-1}(\tilde{p}_a, \tilde{p}_b; \tilde{p}_1, \ldots, \tilde{p}_{j-1}, \tilde{p}_{j+1}, \ldots, \tilde{p}_n)}. \tag{3.14}$$

Eq. (3.14) denotes the single-emission phase space. It can be computed using the lowest possible multiplicity, i.e. $n = 2$ We start from the factorization formula[6]

$$\mathrm{d}\Phi_3(-K; p_i, p_j, Q) = \mathrm{d}\Phi_2(-K; p_j, -n) \frac{\mathrm{d}n^2}{2\pi} \mathrm{d}\Phi_2(-n; p_i, Q), \tag{3.15}$$

where $Q = \sum_{k\neq i,j} p_k$. The two-particle phase space in the frame of a time-like momentum P can be written as

$$\mathrm{d}\Phi_2(p_1 + p_2; p_1, p_2) = \frac{1}{16\pi^2} \frac{\sqrt{(p_1P)^2 - p_1^2P^2}^3}{((p_1P)(p_1p_2) - p_1^2(p_2P))P^2} \mathrm{d}\cos\theta_1^{(P)} \mathrm{d}\phi_1^{(P)}. \tag{3.16}$$

We perform all transformations in the rest frame of n, where we have the simple relations

$$\begin{aligned} E_i &= z\,\frac{-\tilde{p}_i\tilde{K}}{\sqrt{n^2}}, & E_j &= (1-z)\,\frac{-\tilde{p}_i\tilde{K}}{\sqrt{n^2}}, \\ E_K &= (1-z+2\kappa)\,\frac{-\tilde{p}_i\tilde{K}}{\sqrt{n^2}}, \qquad \text{and} \qquad & n^2 &= -2\tilde{p}_i\tilde{K}\,(1-z+\kappa). \end{aligned} \tag{3.17}$$

Using the following identity for the polar angle θ_j of the emission,

$$1 - \cos\theta_j^i = 2v\,\frac{1-z+\kappa}{1-z}, \tag{3.18}$$

we find the first two-particle decay phase space in eq. (3.15) to be

$$\mathrm{d}\Phi_2(-K; p_j, n) = \frac{1}{16\pi^2} \mathrm{d}v\, \mathrm{d}\phi_j^{(n)}. \tag{3.19}$$

Note that this implies that $\phi_j^{(n)}$ is a Lorentz invariant quantity, which is in fact given by eq. (3.10). We also have

$$\mathrm{d}n^2 = -2\tilde{p}_i\tilde{K}\,\mathrm{d}z. \tag{3.20}$$

Finally, we rewrite the second two-particle decay phase space as

$$\mathrm{d}\Phi_2(-n; p_i, Q) = \frac{1}{16\pi^2} \frac{z}{2(1-z+\kappa)} \mathrm{d}\cos\theta_i^{(n)}\, \mathrm{d}\phi_i^{(n)}. \tag{3.21}$$

[6]Note that the n-particle differential phase-space element does not depend on the initial-state momenta individually, hence the notation $\mathrm{d}\Phi_n(p_a, p_b; \ldots)$ is equivalent to $\mathrm{d}\Phi_n(p_a + p_b; \ldots)$.

JHEP10(2023)091

In order to obtain a factorization formula, this must be mapped to the Born phase space, which is given by $\mathrm{d}\Phi_2(-\tilde{K};\tilde{p}_i,\tilde{Q})$. The angular integrals in eq. (3.21) are identical when working in the rest frame of the momentum n, which leads to the relation

$$\mathrm{d}\Phi_2(-n;p_i,Q) = z\,\mathrm{d}\Phi_2(-\tilde{K};\tilde{p}_i,\tilde{Q})\,. \tag{3.22}$$

Combining all of the above, we find the single-emission phase space element

$$\mathrm{d}\Phi^{(\mathrm{FI})}_{+1}(-\tilde{K};\tilde{p}_1,\ldots,\tilde{p}_{j-1},\tilde{p}_{j+1},\ldots,\tilde{p}_n;p_j) = \frac{-2\tilde{p}_i\tilde{K}}{16\pi^2}\,\mathrm{d}v\,\mathrm{d}z\,z\,\frac{\mathrm{d}\phi}{2\pi}\,. \tag{3.23}$$

We derive the analogous factorization formulae for recoilers in the final state and for initial-state emitters in appendix B.

4 Details of the algorithm

This section introduces the details needed to implement our new parton-shower algorithm. The procedure rests on the fact that the angular radiator function $(1-\cos\theta^i_j)\bar{W}^i_{ik,j}$, with $\bar{W}^i_{ik,j}$ given in eq. (2.9), has a fairly mild dependence on the azimuthal angle. In particular, it is finite in the physical domain $0<\theta^i_j,\theta^i_k<\pi$. We can therefore generate the azimuthal angle using a flat prior distribution, and work with standard algorithms for the remainder of the parton shower. In the following, we will assume some familiarity of the reader with these algorithms. Details can be found in the many excellent reviews in the literature, for example [80, 82].

4.1 Soft evolution

We determine energies and angles in a global frame, which is defined by n. In the soft limit, $p_j\to 0$, this frame coincides with the event frame, defined by K. The energies of particles i and j are given by eq. (3.17). The polar angle θ^i_j of the emission is determined by eq. (3.18).[7] We define partial radiator functions, $\bar{w}^i_{ik,j}$, analogous to eq. (2.9), such that $w_{ik,j}=\bar{w}^i_{ik,j}+\bar{w}^k_{ki,j}$. This leads to

$$\bar{w}^i_{ik,j} = \frac{\bar{W}^i_{ik,j}}{E_j^2} = \frac{\bar{W}_{ik,j}}{p_ip_j}\,, \qquad \text{where} \qquad \bar{W}_{ik,j} = \frac{z}{1-z}\,(1-\cos\theta^i_j)\,\bar{W}^i_{ik,j}\,. \tag{4.1}$$

The function $\bar{W}_{ik,j}$ describes the frame-dependent azimuthal modulation of the radiation pattern. We implement it in the numerically more convenient form (see also appendix C)

$$\bar{W}_{ik,j} = \frac{l_{ik}p_i}{l_{ik}p_j}\,, \qquad \text{where} \qquad l^\mu_{ik} = \frac{p^\mu_i}{p_in} + \frac{p^\mu_k}{p_kn}\,. \tag{4.2}$$

The function $(1-\cos\theta^i_j)\bar{W}^i_{ik,j}$ assumes its maximum for $\phi^i_{jk}=0$. It is bounded from above by 2. The eikonal part of the splitting function can therefore be overestimated by

$$\bar{w}^i_{ik,j} \le 2w^{(\mathrm{coll})}_{ik,j}(z) = \frac{1}{2p_ip_j}\,\frac{4z}{1-z}\,. \tag{4.3}$$

[7] Note that for the first emission off a two-parton final state, $\kappa=-1$, such that $1-\cos\theta^i_j = 2v\,z/(1-z)$, which is the same result as in the coherent branching formalism [83].

JHEP10(2023)091

We define the evolution variable of the parton shower as

$$t = 2E_j^2\,(1-\cos\theta_j^i) = v\,(1-z)\,2\tilde{p}_i\tilde{K}\,. \tag{4.4}$$

Note that $1-\cos\theta_j^i = 2\sin^2(\theta_j^i/2)$, such that t corresponds to a transverse momentum. In the generalized rescaling limit $\rho \to 0$ of [84] (see eq. (5.8) and section 5.1 for details), it can be identified with the transverse momentum squared in the Lund plane, hence our parton shower algorithm corresponds to the case $\beta_{\text{PS}} = 0$ in [54]. The kinematical variable v is given as a function of t by

$$v = \frac{\tau}{1-z}\,, \qquad \text{where} \qquad \tau = \frac{t}{2\tilde{p}_i\tilde{K}}\,. \tag{4.5}$$

There is no Jacobian factor for the transformation $\ln v \to \ln t$. The differential branching probability for soft radiation is eventually given by the manifestly Lorentz invariant expression

$$\mathrm{d}P_{ik,j}^{i\,(\text{soft})}(t,z,\phi) = \mathrm{d}\Phi_{+1}(\{\tilde{p}\},p_j)\,8\pi\alpha_s\,C_i\,\bar{w}_{ik,j}^i = \mathrm{d}t\,\mathrm{d}z\,\frac{\mathrm{d}\phi}{2\pi}\,\frac{\alpha_s}{2\pi\,t}\,2C_i\,\bar{W}_{ik,j}\,. \tag{4.6}$$

For any $|\tau| > \tau_0 = t_0/2\tilde{p}_i\tilde{K}$, with t_0 the infrared cutoff of the parton shower, eq. (4.4) defines a boundary on z that is given by $z_+ = 1/(1+\tau_0)$. This regularizes the integral of the overestimate of the splitting function in eq. (4.3). We also introduce a lower bound on z, given by $z_-^2 = t_0/\tilde{K}^2$, to render the upper bound of the t integration finite. This is analogous to the determination of the upper photon energy bound in [85]. The splitting variable z can therefore be generated using standard Monte-Carlo techniques.

4.2 Collinear evolution

We are now left with the task to define the parton-shower algorithm to resum purely collinear logarithms. The corresponding splitting functions can be derived by subtracting the collinear limit of the soft eikonal factor, eq. (2.3), from the leading-order DGLAP splitting functions, eq. (2.13). The differential branching probability for collinear radiation is then given by (see eq. (2.14))

$$\begin{aligned}
\mathrm{d}P_{ik,j}^{i\,(\text{coll})}(t,z,\phi) &= \mathrm{d}\Phi_{+1}(\{\tilde{p}\},p_j)\,\frac{\alpha_s}{2\pi}\left(\frac{P_{\tilde{\imath}i}(z)}{2p_ip_j} - \delta_{\tilde{\imath}i}\,2C_i\,w_{ik,j}^{(\text{coll})}(z)\right) \\
&= \mathrm{d}t\,\mathrm{d}z\,\frac{\mathrm{d}\phi}{2\pi}\,\frac{\alpha_s}{2\pi\,t}\left(P_{\tilde{\imath}i}(z) - \delta_{\tilde{\imath}i}\,C_i\,\frac{2z}{1-z}\right) \\
&= \mathrm{d}t\,\mathrm{d}z\,\frac{\mathrm{d}\phi}{2\pi}\,\frac{\alpha_s}{2\pi\,t}\,C_{\tilde{\imath}i}\,.
\end{aligned} \tag{4.7}$$

Here we have defined the purely collinear remainder functions

$$\begin{aligned}
C_{qq} &= C_F\,(1-z)\,, \\
C_{gg} &= C_A\,z(1-z)\,, \\
C_{gq} &= T_R\,(1-2z(1-z))\,.
\end{aligned} \tag{4.8}$$

While we use the same ordering parameter as in soft evolution, eq. (4.4), an ordering in virtuality or other variables is possible without affecting the logarithmic precision.

JHEP10(2023)091

5 Analysis of logarithmic structure

In this section we will analyze the logarithmic structure of the new parton-shower algorithm. We first provide an analytic proof that the recoil effects from new emissions on pre-existing ones vanish in the $\rho \to 0$ limit [84]. This limit corresponds to a similarity transformation in the Lund plane such that all emissions can be considered as soft or collinear. The technique was introduced to eliminate corrections from kinematic effects which would generate terms beyond NLL accuracy. Parton showers that create non-vanishing recoil effects in this limit are not NLL accurate [53]. Here we focus solely on the question whether the generalized scaling of emissions introduced in [84] is maintained in our parton shower when additional splittings are generated at lower or commensurate scales. In addition, we perform a numerical test of NLL accuracy, following the proposal in [54], which provides an additional strong check of our new algorithm.

5.1 Recoil effects in the infrared limit

We will first show that the new kinematics mapping satisfies the fixed-order criteria for NLL accuracy laid out in [53, 54] to all orders. Proofs for other parton-shower algorithms have been provided in numerical form [54], or based on approximations of the parton-shower branching probability, combined with analytical integration for specific observables [70, 86]. Here we will follow a different approach. We describe the case of pure final-state evolution (for example in $e^+e^- \to$hadrons), similar arguments apply to initial-state evolution as well.

We follow [84] and denote the momenta of the hard partons as $p_1, \ldots, p_n$. Additional soft emissions are denoted by k, and the observable we wish to compute by v. In general, the observable will be a function of both the hard and the soft momenta, $v = V(\{p\}, \{k\})$, while in the soft approximation it reduces to a function of the soft momenta alone, $v = V(\{k\})$. In the rest frame of two hard legs, i and j, one may parametrize the momentum of a single emission as

$$k = z_{i,j} p_i + z_{j,i} p_j + k_{T,ij}\,, \qquad \text{where} \qquad k_{T,ij}^2 = 2 p_i p_j\, z_{i,j}\, z_{j,i}\,. \tag{5.1}$$

The rapidity of the emission in this frame can be parametrized as $\eta_{ij} = 1/2 \ln(z_{i,j}/z_{j,i})$. The observable, computed as a function of the momentum k, radiated collinear to the hard parton, l, can then be expressed as

$$V(k) = \left(\frac{k_{T,l}}{Q}\right)^a e^{-b_l \eta_l}\,, \tag{5.2}$$

where, in the collinear limit, we have $k_{T,l} = k_{T,lj}$ and $\eta_l = \eta_{lj}$ for any $j \nparallel l$.

The cumulative cross section for an arbitrary observable, v, is defined as

$$\Sigma\,(v) := \frac{1}{\sigma} \int^v d\bar{v}\, \frac{d\sigma}{d\bar{v}}\,. \tag{5.3}$$

It is typically decomposed into a Sudakov factor, $e^{-R(v)}$, and a remainder function, $\mathcal{F}(v)$,

$$\Sigma(v) = e^{-R(v)} \mathcal{F}(v)\,. \tag{5.4}$$

JHEP10(2023)091

The remainder function contains no leading logarithms, and the Sudakov radiator is a sum over all partons in the hard process, $R = \sum_l R_l$. The function $\mathcal{F}(v)$ is extracted from the all-orders resummed result, eq. (2.34) of [84], which reads

$$\begin{aligned}\Sigma(v) = &\int \mathrm{d}^3k_1 |M(k_1)|^2 \exp\left\{-\int_{\varepsilon v_1} \mathrm{d}^3k |M(k)|^2\right\} \\ &\times \sum_{m=0}^{\infty} \frac{1}{m!}\Big(\prod_{i=2}^{m+1} \int_{\varepsilon v_1}^{v_1} \mathrm{d}^3k_i |M(k_i)|^2\Big)\Theta\Big(v - V(\{p\}, k_1, \ldots, k_n)\Big)\,.\end{aligned} \tag{5.5}$$

A Taylor expansion in the virtual corrections up to first order in the derivative of the Sudakov radiator, using a cutoff parameter, ε, leads to

$$\exp\left\{-\int_{\varepsilon v_1} \mathrm{d}^3k |M(k)|^2\right\} = e^{-R(v)}\, e^{-R' \ln \frac{v}{\varepsilon v_1} + \mathcal{O}(R'')}\,, \quad \text{where} \quad R' = \frac{\mathrm{d}R}{\mathrm{d}\ln 1/v}\,. \tag{5.6}$$

The function $M(k)$ is the single-emission matrix element in the infrared limit. This leads to the convenient form (cf. eq. (2.37) in [84])

$$\mathcal{F}(v) = \int \mathrm{d}^3k_1 |M(k_1)|^2\, e^{-R' \ln \frac{v}{\varepsilon v_1}} \sum_{m=0}^{\infty} \frac{1}{m!}\Big(\prod_{i=2}^{m+1} \int_{\varepsilon v_1}^{v_1} \mathrm{d}^3k_i |M(k_i)|^2\Big)\Theta\big(v - V(\{p\}, k_1, \ldots, k_n)\big)\,. \tag{5.7}$$

Here, v_1 is the value of the observable in the leading (in v) emission, and k_1 is the corresponding momentum. The expressions to the left of the sum can be interpreted as the differential radiation probability for the first emission, and the corresponding Sudakov suppression factor, assuming that further radiation is resolved down to a scale of εv_1. The sum then implements the corresponding real radiative corrections to all orders, while the Θ function accounts for the constraint from the observable, v. This makes it clear that the $\mathcal{F}$ function is due to multiple emission effects.

In order to cleanly extract the NLL expression for $\mathcal{F}(v)$, the limit $\varepsilon \to 0$ must be taken, and the sum over emissions must be computed to all orders. This corresponds to the limit $\alpha_s \to 0$ or $v \to 0$, while $\alpha_s \ln 1/v$ remains constant. The case $v \to 0$ can be understood as the limit of infinite center-of-mass energy. In this limit, kinematic edge effects can be neglected. However, it must be guaranteed that the event topology in the limit remains the same as in a situation with finite v, which implies that the observable must satisfy the recursive IRC safety conditions laid out in section 2.2.3 of [84]. If it does, one will be able to take the limit and compute $\mathcal{F}(v)$ by performing a similarity transformation in the Lund plane, which is given in terms of a scaling parameter, ρ, by eq. (2.39) of [84]

$$k_{t,l} \to k'_{t,l} = k_{t,l}\rho^{(1-\xi_l)/a + \xi_l/(a+b)}\,, \qquad \eta_l \to \eta'_l = \eta - \xi_l \frac{\ln \rho}{a+b}\,, \qquad \text{where} \qquad \xi = \frac{\eta}{\eta_{\max}}\,. \tag{5.8}$$

This transformation is sketched in figure 3 of [84]. The aim of our proof is to show that the recoil arising from the inverse of the Lorentz transformation in eq. (3.11) does not lead to an appreciable alteration of the momenta of pre-existing emissions in the limit

JHEP10(2023)091

where the scaling parameter vanishes, $\rho \to 0$.[8] In order to analyze the behavior of the Lorentz transformation, we switch back to our original notation and use eq. (3.7) to split K^μ into its components along the recoil momentum, $\tilde{K}^\mu$, the emitter momentum, $\tilde{p}_i^\mu$, and the emission, p_j^μ,

$$K^\mu = \tilde{K}^\mu - X^\mu\,, \qquad \text{where} \qquad X^\mu = p_j^\mu - (1-z)\,\tilde{p}_i^\mu\,. \tag{5.9}$$

The vector X^μ will tend to zero in both the soft and the collinear limit, because it has no component along the direction of the emitter momentum, $\tilde{p}_i$. This implies in particular that for emissions off the original hard partons, X^μ will tend to zero, even in the hard collinear region, such that the Lorentz transformation vanishes. In terms of $\tilde{K}^\mu$ and X^μ, eq. (3.11) takes the form

$$\Lambda^\mu_{\ \nu}(K,\tilde{K}) = g^\mu_\nu + \tilde{K}^\mu A_\nu + X^\mu B_\nu\,, \tag{5.10}$$

where

$$A^\nu = 2\left[\frac{(\tilde{K}-X)^\nu}{(\tilde{K}-X)^2} - \frac{(\tilde{K}-X/2)^\nu}{(\tilde{K}-X/2)^2}\right], \qquad \text{and} \qquad B^\nu = \frac{(\tilde{K}-X/2)^\nu}{(\tilde{K}-X/2)^2}\,. \tag{5.11}$$

Following section 2.2.3 of [84], we now analyze the behavior of this change under the generalized rescaling of all emissions, p_l, according to eq. (5.8). Note that the transverse momentum k_t in this analysis is not the same as $\mathrm{k}_\perp$ in eq. (3.7). It is instead given in terms of Lund plane coordinates, see section 2 of [84] for details of these definitions. We can choose to use the initial momenta of the hard quark and anti-quark (which are not subject to the rescaling) as reference directions to define the Lund plane transverse momentum and rapidity, and work in their rest frame with the quark (antiquark) momentum pointing along the positive (negative) z direction. In this frame, the longitudinal components of the momenta p_l scale as $\tilde{p}_l^{0,3} \sim \rho^{(1-\xi_l)/a}$, while the transverse components behave as $\tilde{p}_l^{1,2} \sim \rho^{(1-\xi_l)/a+\xi_l/(a+b)}$.

From eq. (5.9) we deduce that all components of X^μ scale as the soft momenta $\tilde{p}_l$ in eq. (5.8), because the component of p_j along the emitter momentum $\tilde{p}_i$ has been subtracted. This is a very important feature of our kinematics mapping. We will now show that this mapping maintains the scaling properties, eq. (5.8), of an arbitrary set of pre-existing emissions in the $\rho \to 0$ limit.

First we take the $\rho \to 0$ limit of the coefficients in eq. (5.10). The leading contributions are given by

$$A^\nu \xrightarrow{\rho\to 0} 2\,\frac{\tilde{K}X}{\tilde{K}^2}\,\frac{\tilde{K}^\nu}{\tilde{K}^2} - \frac{X^\nu}{\tilde{K}^2}\,, \qquad \text{and} \qquad B^\nu \xrightarrow{\rho\to 0} \frac{\tilde{K}^\nu}{\tilde{K}^2}\,. \tag{5.12}$$

The momentum shift of particle l under the Lorentz transformation is then given by

$$\Delta p_l^\mu = 2\,\frac{\tilde{K}X}{\tilde{K}^2}\,\frac{\tilde{p}_l\tilde{K}}{\tilde{K}^2}\,\tilde{K}^\mu - \frac{\tilde{p}_l X}{\tilde{K}^2}\,\tilde{K}^\mu + \frac{\tilde{p}_l\tilde{K}}{\tilde{K}^2}\,X^\mu\,. \tag{5.13}$$

[8] In the case of e^+e^- →hadrons, eq. (3.11) is applied to move the initial-state momenta of the e^+e^- collision to a new frame. Afterwards, eq. (A.6) is applied to restore the complete event to the lab frame. As eq. (A.6) in this case is the inverse of eq. (3.11), this corresponds to applying the inverse of eq. (3.11) to the complete final state directly. All other scenarios can be treated in the same fashion for the purpose of this proof.

JHEP10(2023)091

For color singlet decay or production processes we can work in the multipole center-of-mass frame. $\tilde{K}$ then only has an energy component, which is not rescaled as $\rho \to 0$. Let us first assume that the emitter momentum, $\tilde{p}_i$, is one of the soft momenta.

The scaling of the scalar products in eq. (5.13) is then given by[9]

$$\begin{aligned} \tilde{p}_l \tilde{K} &\sim \rho^{(1-\xi_l)/a}\,, \\ \tilde{p}_l X &\sim \rho^{(2-\xi_l-\max(\xi_i,\xi_j))/a}\,. \end{aligned} \tag{5.14}$$

The denominators in A^ν and B^ν do not scale with ρ. With that we can derive the scaling of the change in each component of p_l and compare it to the scaling of the original components in $\tilde{p}_l$.

$$\begin{aligned} \tilde{p}_l^0 &\sim \rho^{(1-\xi_l)/a} \\ \Delta p_l^0 &\sim \rho^{(1-\xi_l)/a} X^0 + \rho^{(2-\xi_l-\max(\xi_i,\xi_j))/a} \tilde{K}^0 + \rho^{(1-\xi_l)/a} X^0 \sim \rho^{(2-\xi_l-\max(\xi_i,\xi_j))/a}\,, \\ \tilde{p}_l^3 &\sim \rho^{(1-\xi_l)/a} \\ \Delta p_l^3 &\sim \rho^{(1-\xi_l)/a} X^3 \sim \rho^{(2-\xi_l-\max(\xi_i,\xi_j))/a}\,, \\ \tilde{p}_l^{1,2} &\sim \rho^{(1-b/(a+b)\xi_l)/a} \\ \Delta p_l^{1,2} &\sim \rho^{(1-\xi_l)/a} X^{1,2} \sim \rho^{(2-\xi_l-b/(a+b)\max(\xi_i,\xi_j))/a}\,. \end{aligned} \tag{5.15}$$

The relative momentum shifts are

$$\begin{aligned} \frac{\Delta p_l^{0,3}}{p_l^{0,3}} &\sim \rho^{(1-\max(\xi_i,\xi_j))/a}\,, \\ \frac{\Delta p_l^{1,2}}{p_l^{1,2}} &\sim \rho^{(1-\xi_l-b/(a+b)(\max(\xi_i,\xi_j)-\xi_l))/a} < \rho^{(1-b/(a+b))(1-\xi_l)/a}\,. \end{aligned} \tag{5.16}$$

If $\xi_l < 1$ and $\max(\xi_i, \xi_j) < 1$, these changes vanish in the $\rho \to 0$ limit. The case of $\xi_l = 1$ and/or $\max(\xi_i, \xi_j) = 1$ corresponds to a phase-space region of measure zero and does therefore not need to be considered.

In the case where $\tilde{p}_i$ is one of the hard momenta, the leading terms in eq. (5.9) cancel exactly, and the remaining components of X^μ are transverse or anti-collinear, leading to a scaling with $\rho^{1/a}$ and $\rho^{2/a}$, respectively, in eq. (5.15). This leads to the same conclusions as the case $\xi_i = \xi_j = 0$.

5.2 Numerical tests of kinematics mapping

In this section we present numerical tests of our new algorithm.[10] We follow the procedure outlined in [54] and perform a scaling of the strong coupling, while keeping the variable $\lambda = \alpha_s \ln v$ fixed, where v is an observable whose single-emission contribution to a measurement

[9] Note that $\tilde{p}_l X$ has two contributions, one proportional to $\rho^{(2-(\xi_l+\max(\xi_i,\xi_j)))/a}$, and one proportional to $\rho^{(2-b/(a+b)(\xi_l+\max(\xi_i,\xi_j)))/a}$. The first one dominates in all cases, because $b/(a+b) < 1$. While b can be negative, infrared and collinear safety requires $b > -a$, $a > 0$.

[10] The PyPy code for these tests can be found at https://gitlab.com/shoeche/pyalaric.

JHEP10(2023)091

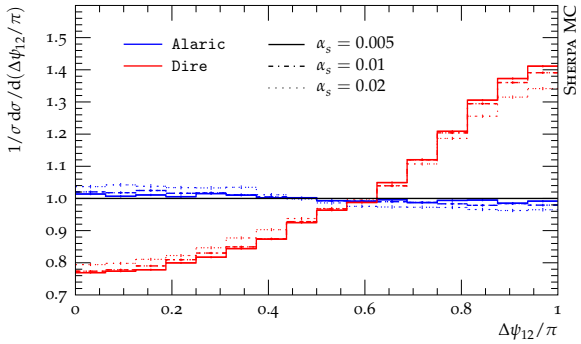

Figure 3. NLL test for $\Delta\psi_{12}$.

can be parametrized in the form $v(k) = (k_t/Q)^a e^{-b|\eta_k|}$, see eq. (5.2). In particular we analyze the event shape observables thrust, T [87], jet broadening, B_T [88], heavy jet mass, M_H, and the fractional energy correlators $FC_{1-\beta}$ [84] for $\beta = 0$ and $1/2$. We also analyze the leading Lund plane declustering scale in the Cambridge algorithm, y_{23}, and the azimuthal angle between the two leading Lund plane declusterings, $\Delta\psi_{12}$ [54].

Since the running of the strong coupling will not affect the kinematics reconstruction, we keep α_s constant in this numerical test. In addition, we do not use the CMW scheme, and we work in the strict leading color approximation, $2C_F = C_A = 3$. We find that this is sufficient to reproduce the dominant features of the DIRE dipole shower algorithm that were observed to break NLL precision in [53, 54]. Figure 3 shows the azimuthal angle separation $\Delta\psi_{12}$. The predictions from DIRE exhibit the same features as already shown in [54], and it can be seen that the deviation from a flat $\Delta\psi_{12}$ distribution does not vanish as $\alpha_s \to 0$. In contrast, for the ALARIC algorithm we observe increasingly smaller deviations from a flat $\Delta\psi_{12}$ dependence, in agreement with NLL resummation.

Figure 4 displays the event shape observables and the leading Lund declustering scale for varying α_s. In order to test for a variety of possible effects of NLL violation, we have chosen observables with different NLL contributions. In addition, we test observables with $b = 0$ ($\sqrt{y_{23}}$, B_T and FC_1), observables with $b = 1/2$ ($FC_{1/2}$) and observables with $b = 1$ ($1 - T$, M_H). In each case we find that the deviation of the ALARIC prediction from the NLL target result (modified to account for constant α_s, no CMW rescaling and leading color) decreases in size proportional to the scaling in α_s, as $\alpha_s \to 0$. At the same time, we observe large deviations of the DIRE predictions from the target NLL result. It is notable that the predictions from ALARIC are flat with respect to the NLL result starting at fairly small values of $-\lambda$ for most observables. For each prediction we have performed a fit to a linear function of α_s in order to extract the limit for $\alpha_s \to 0$. There are two noteworthy artefacts of this extrapolation: Firstly, there are bumps in the extrapolated result at large values of λ, which would not be present in the true ratio at any $\alpha_s < 0.0025$. Second, the extrapolated result is smoother than the individual inputs, since the predictions at smaller α_s are less constraining due to their larger uncertainties. This concludes our tests of the kinematics mapping.

JHEP10(2023)091

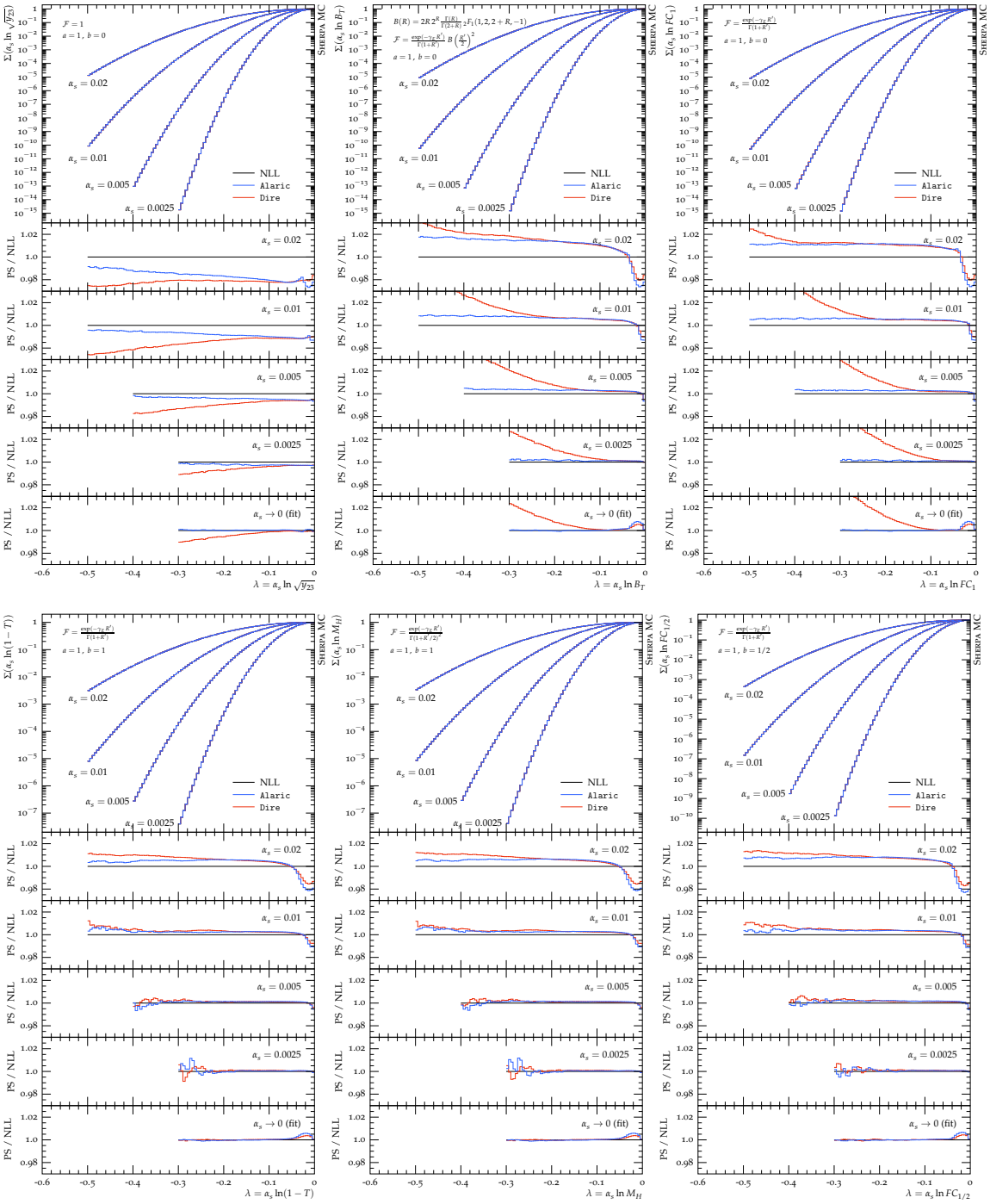

Figure 4. NLL test for various event shape observables. See the main text for details.

JHEP10(2023)091

6 Comparison to experimental data

In this section we present first numerical results obtained with the Alaric final-state parton shower, as implemented in the event generation framework Sherpa [75–77]. We do not perform NLO matching or multi-jet merging, and we set $C_F = (N_c^2 - 1)/(2N_c) = 4/3$ and $C_A = 3$. All quarks are considered massless, and we implement flavor thresholds at $m_c = 1.42\,\text{GeV}$ and $m_b = 4.92\,\text{GeV}$. The running coupling is evaluated at two loop accuracy, and we set $\alpha_s(m_z) = 0.118$. Following standard practice to improve the logarithmic accuracy of the parton shower, we employ the CMW scheme [91], i.e. the soft eikonal contribution to the flavor conserving splitting functions is rescaled by $1+\alpha_s(t)/(2\pi)K$, where $K = (67/18 - \pi^2/6)\,C_A - 10/9\,T_R\,n_f$. Our results include the simulation of hadronization using the Lund string fragmentation implemented in Pythia 6.4 [82].[11] We use the default hadronization parameters, apart from the following values: `PARJ(21)=0.3`, `PARJ(41)=0.4`, `PARJ(42)=0.36` for Alaric, and `PARJ(21)=0.3`, `PARJ(41)=0.4`, `PARJ(42)=0.45` for Dire. All analyses are performed with Rivet [93].

Figure 5 shows predictions from the Alaric parton shower for differential jet rates in the Durham scheme compared to experimental results from the JADE and OPAL collaborations [89]. The perturbative region is to the right of the plot, and $y \sim 2.8 \cdot 10^{-3}$ corresponds to the b-quark mass. The simulation of nonperturbative effects dominates the predictions below $\sim 10^{-4}$. We observe fairly good agreement with the experimental data, however, we note that at moderate values of y the prediction will be altered when a proper evolution of massive quark final states is included.

Figure 6 shows a comparison for event shapes measured by the ALEPH collaboration [90]. The perturbative region is to the right of the plot, except for the thrust distribution, where it is to the left. We notice some deviation in the predictions for the total jet broadening and for the aplanarity. They are mostly within the 2σ uncertainty of the experimental measurements. It can be expected that the simulations will improve upon including matrix-element corrections or when merging the Alaric parton shower with higher-multiplicity calculations. Deviations in the hadronization region may be associated with the treatment of b-quarks and c-quarks as massless partons.

7 Conclusions

We have presented a new parton-shower algorithm, which is closely modeled on the fixed-order subtraction formalism for identified particles by Catani and Seymour. This technique allows, for the first time in a dipole-like parton shower, to disentangle color and kinematics, at the price of introducing an azimuthal angle dependence in the splitting functions. Partial fractioning the angular radiator function and matching to the collinear limit maintains strict positivity of the evolution kernels, thus allowing a straightforward implementation without the need for explicit angular ordering. Through a suitable assignment of recoil, which

[11] Hadronization using the Sherpa cluster fragmentation [92] will require an implementation of massive splitting functions in Alaric, in order to simulate the QCD evolution of partonic hadron decays. We postpone this to a future publication.

JHEP10(2023)091

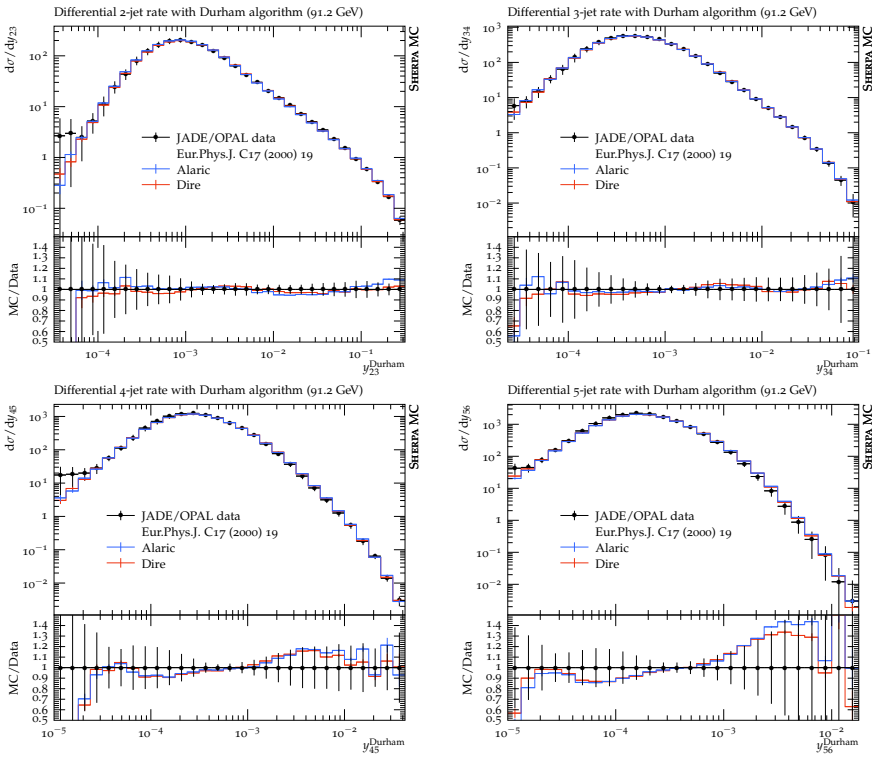

Figure 5. ALARIC and DIRE predictions in comparison to LEP data from [89].

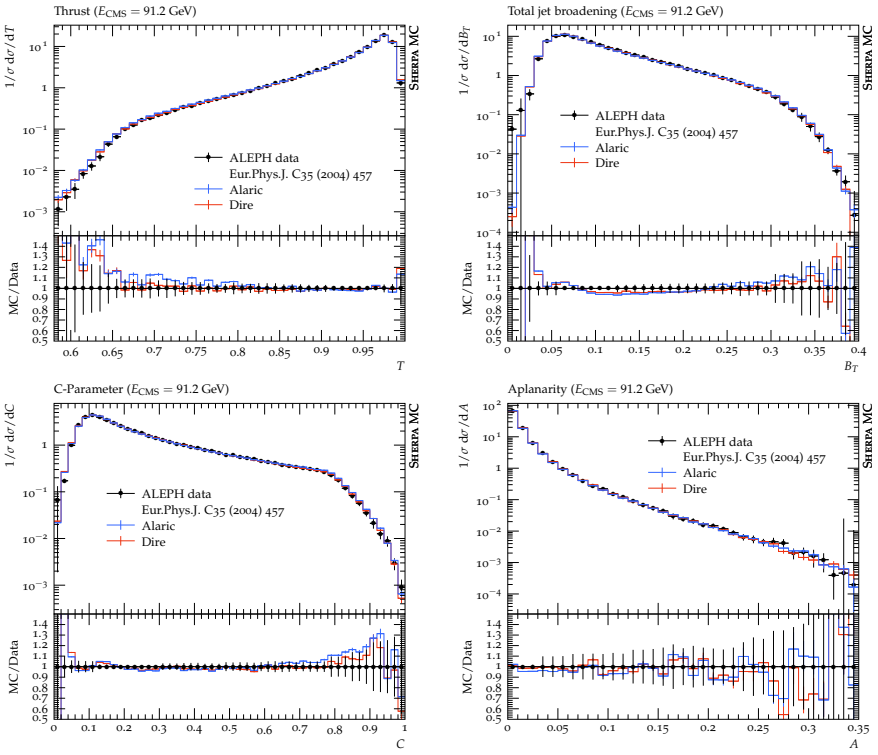

Figure 6. ALARIC and DIRE predictions in comparison to LEP data from [90].

JHEP10(2023)091

is absorbed by the entire QCD multipole, we are able to show that the local kinematics mapping satisfies the criteria for NLL precision.

Several extensions of this algorithm are required: Firstly, it should be modified to include spin correlations [23–26] and dominant sub-leading color effects [67, 74, 94]. A number of formally less relevant, but practically important considerations need to be addressed as well. They include the evolution for massive partons, in order to properly describe bottom and charm jet production and b- and c-quark fragmentation functions. Another open question is the extension to processes with non-trivial color dependence at Born level, such as top-quark pair production and inclusive jet or di-jet production at hadron colliders. A related, though substantially simpler problem is the treatment of processes with multiple, disconnected QCD multipoles, such as vector boson fusion in the structure function approximation, or the production of a Higgs boson in association with a hadronically decaying vector boson in the narrow width approximation. The latter cases can be handled by applying the algorithms introduced here to each QCD multipole individually, while keeping track of spin correlations among the different multipoles. Finally, we plan to extend our new algorithms to higher-orders, based on the techniques developed in [73, 74, 95].

Acknowledgments

We thank Andrea Banfi for pointing out that the relative difference between the parton-shower and the NLL result in figure 4 should decrease proportional to α_s as $\alpha_s \to 0$. The work of F. Herren and S. Höche was supported by the Fermi National Accelerator Laboratory (Fermilab), a U.S. Department of Energy, Office of Science, HEP User Facility. Fermilab is managed by Fermi Research Alliance, LLC (FRA), acting under Contract No. DE–AC02–07CH11359. F. Herren acknowledges support by the Alexander von Humboldt foundation. This work has received funding from the European Union's Horizon 2020 research and innovation programme as part of the Marie Skłodowska-Curie Innovative Training Network MCnetITN3 (grant agreement no. 722104). F. Krauss acknowledges funding as Royal Society Wolfson Research fellow. F. Krauss and M. Schönherr are supported by the STFC under grant agreement ST/P001246/1. They would like to thank the Munich Institute for Astro-, Particle and BioPhysics (MIAPbP), funded by the Deutsche Forschungsgemeinschaft (DFG, German Research Foundation) under Germany's Excellence Strategy – EXC-2094 – 390783311, for hospitality while this publication was finalized. The work of M. Schönherr was supported by the Royal Society through a University Research Fellowship (URF\R1\180549) and an Enhancement Award (RGF\EA\181033, CEC19\100349, and RF\ERE\210397).

A Implementation details

This appendix summarizes details of the kinematics mapping and the relations between the kinematic invariants and the evolution and splitting variables for both final-state and initial-state evolution. We limit the discussion to situations where the recoiler momentum is composed either of final-state momenta only, or of initial-state momenta only.

JHEP10(2023)091

A.1 Final-state evolution

We will first discuss the case of a final-state emitter with a recoil momentum $\tilde{K}$ that is composed only of final-state momenta. The momentum mapping is sketched in figure 7 (FF). The emitting particle is labeled i, the emission is labeled j, and the color spectator is labeled k. The momenta p_i, p_j and K are given by eq. (3.7)

$$\begin{aligned} p_i &= z\,\tilde{p}_i\,, \\ p_j &= (1-z)\,\tilde{p}_i + v\big(\tilde{K} - (1-z+2\kappa)\,\tilde{p}_i\big) + k_\perp\,, \\ K &= \tilde{K} - v\big(\tilde{K} - (1-z+2\kappa)\,\tilde{p}_i\big) - k_\perp\,, \end{aligned} \tag{A.1}$$

where

$$\mathrm{k}_\perp^2 = v(1-v)(1-z)\,2\tilde{p}_i\tilde{K} - v^2\tilde{K}^2\,, \qquad \text{and} \qquad v = \frac{\tau}{1-z}\,. \tag{A.2}$$

The particles included in the momentum $\tilde{K}$ are subjected to a Lorentz transformation, which accounts for the decay of the new recoil momentum, K, in a different frame. If the recoil momentum is given by a single, light-like vector, no such transformation is necessary.

$$p_l^\mu \to \Lambda^\mu_\nu(\tilde{K}, K)\,p_l^\nu\,. \tag{A.3}$$

The momentum mapping for final-state emitters with a recoil momentum $\tilde{K}$ composed only of initial-state momenta is sketched in figure 7 (FI). We define the momentum $\tilde{K}$ as incoming, i.e. $\tilde{K}_0 > 0$. This implies the replacement $v \to -v$, $\tilde{K} \to -\tilde{K}$ and $n \to -n$, leading to

$$\begin{aligned} p_i &= z\,\tilde{p}_i\,, \\ p_j &= (1-z)\,\tilde{p}_i + v\big(\tilde{K} + (1-z-2\kappa)\,\tilde{p}_i\big) + k_\perp\,, \\ K &= \tilde{K} + v\big(\tilde{K} + (1-z-2\kappa)\,\tilde{p}_i\big) + k_\perp\,, \end{aligned} \tag{A.4}$$

where

$$\mathrm{k}_\perp^2 = v(1+v)(1-z)\,2\tilde{p}_i\tilde{K} - v^2\tilde{K}^2\,, \qquad \text{and} \qquad v = \frac{\tau}{1-z}\,. \tag{A.5}$$

As in the case of a final-state spectator, the momenta defining $\tilde{K}$ are subjected to the Lorentz transformation given by eq. (A.3). An additional transformation has to be applied, such as to align the momenta of both redefined beam particles, p_a and p_b, with the beam axis. If there are no strongly interacting particles in the initial state, this can be achieved by the simple mapping

$$p_l^\mu \to \Lambda^\mu_\nu(p_a + p_b, \tilde{p}_a + \tilde{p}_b)\,p_l^\nu\,. \tag{A.6}$$

Note that this additional Lorentz transformation is applied to all particles in the event.

A.2 Initial-state evolution

For initial-state emissions, we redefine $z \to 1/z$. The momentum mapping for recoil momenta $\tilde{K}$ composed only of initial-state momenta is sketched in figure 7 (II). The emitting particle is labeled i, the emission is labeled j, and the color spectator is labeled k.

JHEP10(2023)091

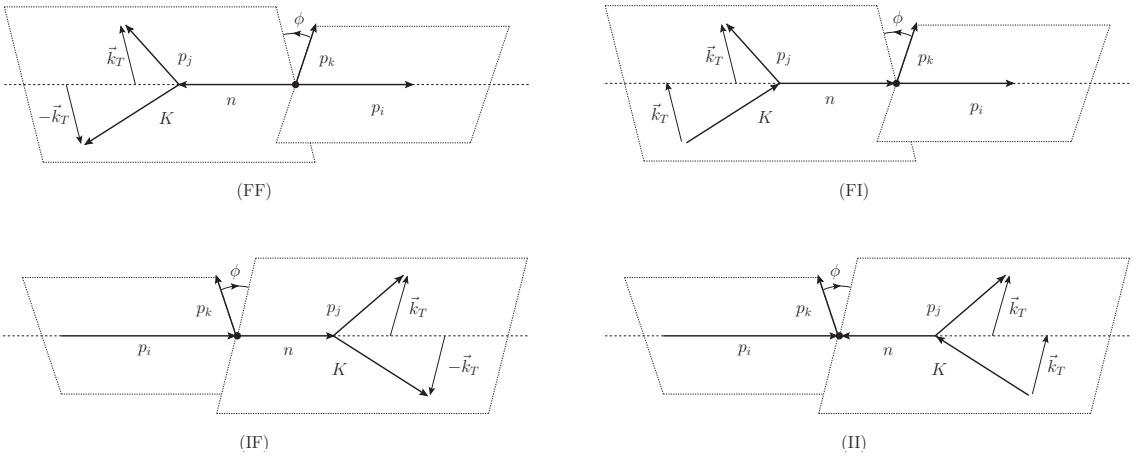

Figure 7. Sketch of the momentum mapping for final-state emitters with final-state spectator (FF), final-state emitters with initial-state spectator (FI), initial-state emitters with final-state spectator (IF) and initial-state emitters with initial-state spectator (II).

We define both $\tilde{p}_i$ and $\tilde{K}$ as incoming, i.e. $\tilde{p}_{i,0} > 0$ and $\tilde{K}_0 > 0$. The momenta p_i, p_j and K are then given by eq. (3.7)

$$\begin{aligned} p_i &= \frac{1}{z}\,\tilde{p}_i\,, \\ p_j &= \frac{1-z}{z}\,\tilde{p}_i + v\left(\tilde{K} + \left(\frac{1-z}{z} - 2\kappa\right)\tilde{p}_i\right) + k_\perp\,, \\ K &= \tilde{K} + v\left(\tilde{K} + \left(\frac{1-z}{z} - 2\kappa\right)\tilde{p}_i\right) + k_\perp\,, \end{aligned} \tag{A.7}$$

where

$$\mathrm{k}_\perp^2 = v(1+v)\frac{1-z}{z}\,2\tilde{p}_i\tilde{K} - v^2\tilde{K}^2\,, \qquad \text{and} \qquad v = \frac{\tau}{1-z}\,. \tag{A.8}$$

As in the case of final-state evolution, the momenta defining $\tilde{K}$ are subjected to the Lorentz transformation given by eq. (A.3). The complete event is then subjected to a Lorentz transformation, determined such as to align the momenta of the initial-state particles, p_a and p_b, with the beam axis, while shifting the event rapidity to $y = \tilde{y} - \mathrm{sgn}(p_{i,z})\ln\sqrt{z}$ and preserving the azimuthal orientation of the event.

The momentum mapping for initial-state emitters with a recoil momentum $\tilde{K}$ composed only of final-state momenta is sketched in figure 7 (IF). The momenta p_i, p_j and K are given by

$$\begin{aligned} p_i &= \frac{1}{z}\,\tilde{p}_i\,, \\ p_j &= \frac{1-z}{z}\,\tilde{p}_i + v\left(\tilde{K} - \left(\frac{1-z}{z} + 2\kappa\right)\tilde{p}_i\right) + k_\perp\,, \\ K &= \tilde{K} - v\left(\tilde{K} - \left(\frac{1-z}{z} + 2\kappa\right)\tilde{p}_i\right) - k_\perp\,, \end{aligned} \tag{A.9}$$

where

$$\mathrm{k}_\perp^2 = v(1-v)\frac{1-z}{z}\,2\tilde{p}_i\tilde{K} - v^2\tilde{K}^2\,, \qquad \text{and} \qquad v = \frac{\tau}{1-z}\,. \tag{A.10}$$

JHEP10(2023)091

The particles included in the momentum $\tilde{K}$ are subjected to a Lorentz transformation, which accounts for the decay of the new recoil momentum, K, in a different frame. As in the case of final-state evolution, this can be achieved by applying the Lorentz transformation in eq. (A.3). If the recoil momentum is given by a single, light-like vector, no transformation is needed.

B Phase-space factorization

This appendix summarizes details on the phase-space factorization for both final-state and initial-state evolution. The case of final-state emitter and initial-state recoiler was discussed in section 3, and we do not repeat it here.

B.1 Final-state emitter and final-state recoiler

This case covers electroweak decays of a color-charged resonance, such as the top quark. We start from

$$\mathrm{d}\Phi_3(p_i, p_j, K; Q) = \mathrm{d}\Phi_2(p_i, n; Q)\,\frac{\mathrm{d}n^2}{2\pi}\,\mathrm{d}\Phi_2(p_j, K; n) \tag{B.1}$$

The generic frame-independent form of the two-particle phase space is given in eq. (3.16). We perform all transformations in the rest frame of n, where we have the simple relations

$$\begin{aligned} E_i &= z\,\frac{\tilde{p}_i\tilde{K}}{\sqrt{n^2}}\,, & E_j &= (1-z)\,\frac{\tilde{p}_i\tilde{K}}{\sqrt{n^2}}\,, \\ E_K &= (1-z+2\kappa)\,\frac{\tilde{p}_i\tilde{K}}{\sqrt{n^2}}\,, \qquad \text{and} \qquad & n^2 &= 2\tilde{p}_i\tilde{K}\,(1-z+\kappa)\,. \end{aligned} \tag{B.2}$$

Using the following identity for the polar angle θ_j of the emission,

$$1-\cos\theta_j^i = -2v\,\frac{1-z+\kappa}{1-z}\,, \tag{B.3}$$

we find the first two-particle decay phase space to be

$$\mathrm{d}\Phi_2(p_j, K; n) = \frac{1}{16\pi^2}\,\mathrm{d}v\,\frac{\mathrm{d}\phi_j^{(n)}}{2\pi}\,. \tag{B.4}$$

Analogous to eq. (3.20), we can write $\mathrm{d}n^2 = 2\tilde{p}_i\tilde{K}\,\mathrm{d}z$. Finally, we rewrite the second two-particle decay phase space

$$\mathrm{d}\Phi_2(p_i, n; Q) = \frac{1}{16\pi^2}\,\frac{z}{2(1-z+\kappa)}\,\mathrm{d}\cos\theta_i^{(n)}\,\frac{\mathrm{d}\phi_i^{(n)}}{2\pi}\,. \tag{B.5}$$

In order to obtain a factorization formula, this must be mapped to the Born phase space, which is given by $\mathrm{d}\Phi_2(\tilde{p}_i, \tilde{K}; Q)$. The angular integrals in eq. (B.5) are identical when working in the rest frame of the momentum n, which leads to the relation $\mathrm{d}\Phi_2(p_i, n; Q) = z\,\mathrm{d}\Phi_2(\tilde{p}_i, \tilde{q}_i; \tilde{K})$. Combining all of the above, we find the single-emission phase space element

$$\mathrm{d}\Phi_{+1}^{(\mathrm{FF})}(\tilde{K}; \tilde{p}_1, \ldots, \tilde{p}_{j-1}, \tilde{p}_{j+1}, \ldots, \tilde{p}_n; p_j) = \frac{2z\tilde{p}_i\tilde{K}}{16\pi^2}\,\mathrm{d}v\,\mathrm{d}z\,\frac{\mathrm{d}\phi}{2\pi}\,. \tag{B.6}$$

JHEP10(2023)091

B.2 Initial-state emitter and final-state recoiler

This case covers hadroproduction of a colorless final state, in particular Drell-Yan lepton pair production. We start from the factorization formula

$$\mathrm{d}\Phi_2(p_j, K; Q + p_i) = \mathrm{d}\Phi_2(p_j, K; n)\, \frac{\mathrm{d}n^2}{2\pi}\, \mathrm{d}\Phi_1(n; Q + p_i) \tag{B.7}$$

The generic frame-independent form of the two-particle phase space is given in eq. (3.16). Again, we perform all transformations in the rest frame of n, leading to the relations in eq. (B.2). Using eq. (B.3) for the polar angle θ_j of the emission, we find the two-particle decay phase space in eq. (B.4). Analogous to eq. (3.20), we can write $\mathrm{d}n^2 = 2\tilde{p}_i\tilde{K}\,\mathrm{d}z$. The one-particle production phase space is given by

$$\mathrm{d}\Phi_1(n; Q + p_i) = 2\pi\, \delta(n^2 - (Q + p_i)^2)\,. \tag{B.8}$$

In order to obtain a factorization formula, this is mapped to the Born phase space, leading to $\mathrm{d}\Phi_1(n; Q + p_i) = 1/z\ \mathrm{d}\Phi_2(\tilde{K}; Q + \tilde{p}_i)$. Combining all of the above, we obtain the single-emission phase space element

$$\mathrm{d}\Phi_{+1}^{(\mathrm{IF})}(\tilde{K}; \tilde{p}_1, \ldots, \tilde{p}_{j-1}, \tilde{p}_{j+1}, \ldots, \tilde{p}_n; p_j) = \frac{2\tilde{p}_i\tilde{K}}{16\pi^2}\, \mathrm{d}v\, \frac{\mathrm{d}x}{x}\, \frac{\mathrm{d}\phi}{2\pi}\,. \tag{B.9}$$

B.3 Initial-state emitter and initial-state recoiler

This case covers deep inelastic scattering. We start from the two-particle phase space

$$\mathrm{d}\Phi_2(p_j, Q; K + p_i)\,. \tag{B.10}$$

Its generic, frame-independent form is given in eq. (3.16). We perform all transformations in the rest frame of n, where we have the relations in eq. (3.17). Next we insert the identity

$$\begin{aligned} 1 &= \int \mathrm{d}x\ \delta\left(x - \frac{\tilde{p}_i\tilde{K}}{p_i n}\right) = \int \mathrm{d}x\ \frac{2\tilde{p}_i\tilde{K}}{x}\ \delta\left(2\tilde{p}_i\tilde{K} - (p_i + p_j)n\right) \\ &= \int \mathrm{d}x\ \frac{2\tilde{p}_i\tilde{K}}{x}\ \delta\left((\tilde{p}_i + \tilde{K})^2 - Q^2\right)\,. \end{aligned} \tag{B.11}$$

In order to obtain a factorization formula, this is mapped to the Born phase space as $\mathrm{d}\Phi_1(\tilde{Q}; \tilde{p}_i + \tilde{K}) = 2\pi\, \delta(\tilde{Q}^2 - (\tilde{p}_i + \tilde{K})^2)$. Combining all of the above, we obtain the single-emission phase space element

$$\mathrm{d}\Phi_{+1}^{(\mathrm{IF})}(\tilde{K}; \tilde{p}_1, \ldots, \tilde{p}_{j-1}, \tilde{p}_{j+1}, \ldots, \tilde{p}_n; p_j) = \frac{2\tilde{p}_i\tilde{K}}{16\pi^2}\, \mathrm{d}v\, \frac{\mathrm{d}x}{x}\, \frac{\mathrm{d}\phi}{2\pi}\,. \tag{B.12}$$

C Monte-Carlo counterterms for MC@NLO matching

To match a parton shower to NLO calculations in dimensional regularization based on the MC@NLO algorithm [27], the integral of the splitting functions must be known in $D = 4 - 2\varepsilon$ dimensions. Since our new parton shower is modeled on the Catani-Seymour identified particle subtraction, we can utilize the techniques developed in [96, 97]. By

JHEP10(2023)091

means of a suitable identification of the radiating color multipole, this allows us to treat the problem of standard final-state evolution, resonant particle production, color singlet production at hadron colliders, deep-inelastic scattering, etc. on the same footing.

Here we will limit ourselves to listing the main changes with respect to [96, 97] that are needed in order to implement the algorithm. For details on the respective phase-space integrals, and on the basis of the subtraction technique, we refer the reader to [72]. Details on the implementation of MC@NLO can be found in [27, 32].

C.1 Final-state emitter

By combining the integrated splitting function with the collinear mass factorization counterterms, we can derive a combined integrated subtraction term for identified parton production with a partonic fragmentation function [96, 97]

$$\int_{m+1} \mathrm{d}\sigma^S + \int_m \mathrm{d}\sigma^C = \frac{1}{2} \sum_{i=g,q,\bar{q}} \sum_{\tilde{\imath}=1}^{m} \int_0^1 \frac{\mathrm{d}z}{z^{2-2\epsilon}} \int_m \mathrm{d}\sigma^B \left(p_1, \ldots, \frac{p_i}{z}, \ldots, p_m\right) \otimes \hat{\mathbf{I}}_{\tilde{\imath}i}^{(\mathrm{FS})}, \quad \text{(C.1)}$$

where the $\otimes$ stands for spin and color correlations. In the $\overline{\mathrm{MS}}$ scheme, the insertion operator is given by

$$\begin{aligned}\hat{\mathbf{I}}_{\tilde{\imath}i}^{(\mathrm{FS})} = &-\frac{\alpha_s}{2\pi} \frac{1}{\Gamma(1-\epsilon)} \\ &\times \left\{ \sum_{k=1,k\neq\tilde{\imath}}^{m} \frac{\mathbf{T}_{\tilde{\imath}} \mathbf{T}_k}{\mathbf{T}_{\tilde{\imath}}^2} \left(\frac{4\pi\mu^2 (p_k n)}{2(p_i p_k)(p_i n)} \right)^{\epsilon} \hat{\mathcal{V}}_{\tilde{\imath},i}(z;\epsilon;p_i,p_k,n) - \delta_{\tilde{\imath}i} \frac{1}{\epsilon} \left(\frac{4\pi\mu^2}{\mu_F^2} \right)^{\epsilon} P_{\tilde{\imath}i}(z) \right\}. \end{aligned} \quad \text{(C.2)}$$

The explicit pole in ϵ, originating from the renormalization of the perturbative fragmentation function, cancels against the corresponding pole in $\bar{\mathcal{V}}_{\tilde{\imath},i}$. The remainder can be split into three contributions:

$$\hat{\mathbf{I}}_{\tilde{\imath}i}^{(\mathrm{FS})} = \delta(1-z)\mathbf{I}_{\tilde{\imath}i} + \mathbf{P}_{\tilde{\imath}i} + \mathbf{H}_{\tilde{\imath}i}\,. \quad \text{(C.3)}$$

The singularities in the virtual corrections are canceled by the insertion operator present for standard final-state dipoles with final-state spectator [72]

$$\mathbf{I}_{\tilde{\imath}i}(p_1,\ldots,p_i,\ldots,p_m;\epsilon) = -\frac{\alpha_s}{2\pi} \frac{1}{\Gamma(1-\epsilon)} \sum_{k=1,k\neq\tilde{\imath}}^{m} \frac{\mathbf{T}_{\tilde{\imath}} \mathbf{T}_k}{\mathbf{T}_{\tilde{\imath}}^2} \left(\frac{4\pi\mu^2 (p_k n)}{2(p_i p_k)(p_i n)} \right)^{\epsilon} \mathcal{V}_{\tilde{\imath}i}(\epsilon)\,. \quad \text{(C.4)}$$

Employing color conservation and expanding through $\mathcal{O}(\epsilon)$, the remaining two operators read [96, 97]

$$\mathbf{P}_{\tilde{\imath}i}(p_1,\ldots,\frac{p_i}{z},\ldots,p_m;z;\mu_F) = \frac{\alpha_s}{2\pi} \sum_{k=1,k\neq\tilde{\imath}}^{m} \frac{\mathbf{T}_{\tilde{\imath}} \mathbf{T}_k}{\mathbf{T}_{\tilde{\imath}}^2} \ln \frac{z^2\mu_F^2 (p_k n)}{2(p_i p_k)(p_i n)} \delta_{\tilde{\imath}i} P_{\tilde{\imath}i}(z) \quad \text{(C.5)}$$

and

$$\begin{aligned}&\mathbf{H}_{\tilde{\imath}i}(p_1,\ldots,p_i,\ldots,p_m;n;z) \\ &\quad = -\frac{\alpha_s}{2\pi} \sum_{k=1,k\neq\tilde{\imath}}^{m} \frac{\mathbf{T}_{\tilde{\imath}} \mathbf{T}_k}{\mathbf{T}_{\tilde{\imath}}^2} \left[\tilde{K}^{\tilde{\imath}i}(z) + \bar{K}^{\tilde{\imath}i}(z) + 2P_{\tilde{\imath}i}(z)\ln z + \hat{\mathcal{L}}^{\tilde{\imath}i}(z;p_i,p_k,n) \right]. \end{aligned} \quad \text{(C.6)}$$

JHEP10(2023)091

Finally, an integration over p_i has to be performed. Following refs. [96, 97] we replace the integration over p_i by an integration over $\tilde{p}_i$. This leads to a Jacobian of $z^{2-2\epsilon}$, canceling the prefactor in eq. (C.1). Consequently, the differential Born cross-section $\mathrm{d}\sigma^B$ decouples from the z integration and we obtain

$$\sum_{\tilde{\imath}=1}^{m} \int \frac{\mathrm{d}^D p_i}{(2\pi)^{D-1}} \delta(p_i^2) \sigma^I(p_i) = \sum_{\tilde{\imath}=1}^{m} \int_m \mathrm{d}\sigma^B(p_1, \ldots, p_m) \otimes \int_0^1 \mathrm{d}z \, \frac{1}{2} \sum_{i=g,q,\bar{q}} \hat{\mathbf{I}}_{\tilde{\imath}i} \,. \tag{C.7}$$

The integral over $\sum_i \mathbf{P}_{\tilde{\imath}i}$ vanishes, because $\sum_i P_{\tilde{\imath}i}$ is a pure plus distribution. The other two z-integrals can be evaluated directly, because $\tilde{p}_i$ is z-independent. In particular, the integral of the $\mathbf{I}_{\tilde{\imath}}$ operator is trivial. The integral over the $\mathbf{H}_{\tilde{\imath}i}$ operator is given by a modified form of the result in [96, 97]. We note that the arguments of the dilogarithms depend only on the angle and velocity of l_{ik} as defined in eq. (4.2), see appendix B in [72]. Using the following substitution in eq. (B.9) in [72][12]

$$1 - v \cos\chi \to \frac{n^2 \, l_{ik} p_i}{(p_i n)(l_{ik} n)} \,, \qquad 1 - v^2 \to \frac{n^2 l_{ik}^2}{(l_{ik} n)^2} \,, \tag{C.8}$$

we therefore obtain

$$\begin{aligned} &\int_0^1 \mathrm{d}z \, \mathbf{H}_{\tilde{\imath}i}(p_1, \ldots, p_i, \ldots, p_m; n; z) \\ &\quad = -\frac{\alpha_s}{2\pi} \sum_{k=1, k\neq\tilde{\imath}}^{m} \frac{\mathbf{T}_{\tilde{\imath}} \mathbf{T}_k}{\mathbf{T}_{\tilde{\imath}}^2} \left\{ \mathcal{K}^{\tilde{\imath}i} + \delta_{\tilde{\imath}i} \, \mathrm{Li}_2\left(1 - \frac{2\tilde{p}_i \tilde{p}_k \tilde{K}^2}{(\tilde{p}_i \tilde{K})(\tilde{p}_k \tilde{K})}\right) - \int_0^1 \mathrm{d}z \, P_{\mathrm{reg}}^{\tilde{\imath}i}(z) \ln \frac{(p_i p_k) n^2}{2(p_i n)(p_k n)} \right\}, \end{aligned} \tag{C.9}$$

where the integral $\mathcal{K}^{\tilde{\imath}i}$ is defined as

$$\mathcal{K}^{\tilde{\imath}i} = \int_0^1 \mathrm{d}z \, \left(\bar{K}^{\tilde{\imath}i}(z) + \tilde{K}^{\tilde{\imath}i}(z) + 2 P_{\tilde{\imath}i}(z) \ln z \right). \tag{C.10}$$

In general, the last term of eq. (C.9) must be computed numerically, as n implicitly depends on z, see eq. (3.3).

C.2 Initial-state emitter

As in the case of a final-state emitter, the case of an initial state emitter is treated in the same manner as in [96, 97]. The sum of the subtraction terms and the collinear counterterms is given by

$$\int_{m+1} \mathrm{d}\sigma^S + \int_m \mathrm{d}\sigma^C = \sum_{\tilde{\imath}=g,q,\bar{q}} \int_0^1 \mathrm{d}x \int_m \mathrm{d}\sigma^B(p_1, \ldots, x p_i, \ldots, p_m) \otimes \hat{\mathbf{I}}_{i\tilde{\imath}}^{(\mathrm{IS})} \,, \tag{C.11}$$

where the $\otimes$ again stands for spin and color correlations. In the $\overline{\mathrm{MS}}$ scheme, the insertion operator is given by

$$\hat{\mathbf{I}}_{i\tilde{\imath}}^{(\mathrm{IS})} = \delta(1-z) \mathbf{I}_{i\tilde{\imath}} + \mathbf{P}_{i\tilde{\imath}} + \mathbf{K}_{i\tilde{\imath}} \,. \tag{C.12}$$

[12] Note that in this context v is defined as the relative velocity of l_{ik} and n, see appendix B in [72].

JHEP10(2023)091

The operator $\mathbf{I}_{i\tilde{\imath}}$ is obtained by replacing $k \to \tilde{k}$ in eq. (C.4). The $\mathbf{K}$ operator can be written as

$$\mathbf{K}_{i\tilde{\imath}}(p_1,\ldots,p_m;p_i,n,x) = -\frac{\alpha_s}{2\pi}\sum_{\tilde{b}=1}^{m}\frac{\mathbf{T}_{\tilde{k}}\mathbf{T}_{\tilde{\imath}}}{\mathbf{T}_{\tilde{\imath}}^2}\left[\,\bar{K}^{i,\tilde{\imath}}(x)+\tilde{K}^{i,\tilde{\imath}}(x)+\mathcal{L}^{i,\tilde{\imath}}(x;p_i,\tilde{p}_k,n)\,\right]. \quad \text{(C.13)}$$

This result can be derived from eq. (C.6) by using the known expressions for the breaking of the Gribov-Lipatov relation at NLO QCD, see section 6.4 of [98]. All remaining components of the subtraction formulae can be found in appendix C of [72].

Open Access. This article is distributed under the terms of the Creative Commons Attribution License (CC-BY 4.0), which permits any use, distribution and reproduction in any medium, provided the original author(s) and source are credited.

JHEP10(2023)091

References

[1] A. Buckley et al., *General-purpose event generators for LHC physics*, *Phys. Rept.* **504** (2011) 145 [arXiv:1101.2599] [INSPIRE].

[2] J.M. Campbell et al., *Event Generators for High-Energy Physics Experiments*, in the proceedings of the *Snowmass 2021*, Washington University, Seattle, WA, U.S.A., 17–26 July 2022, [arXiv:2203.11110] [INSPIRE].

[3] Y.L. Dokshitzer, *Calculation of the Structure Functions for Deep Inelastic Scattering and e^+e^- Annihilation by Perturbation Theory in Quantum Chromodynamics*, *Sov. Phys. JETP* **46** (1977) 641 [INSPIRE].

[4] V.N. Gribov and L.N. Lipatov, *Deep inelastic e p scattering in perturbation theory*, *Sov. J. Nucl. Phys.* **15** (1972) 438 [INSPIRE].

[5] L.N. Lipatov, *The parton model and perturbation theory*, *Yad. Fiz.* **20** (1974) 181 [INSPIRE].

[6] G. Altarelli and G. Parisi, *Asymptotic Freedom in Parton Language*, *Nucl. Phys. B* **126** (1977) 298 [INSPIRE].

[7] L. Lönnblad, *ARIADNE version 4: A program for simulation of QCD cascades implementing the color dipole model*, *Comput. Phys. Commun.* **71** (1992) 15 [INSPIRE].

[8] H. Kharraziha and L. Lönnblad, *The linked dipole chain Monte Carlo*, *JHEP* **03** (1998) 006 [hep-ph/9709424] [INSPIRE].

[9] H. Jung and G.P. Salam, *Hadronic final state predictions from CCFM: The Hadron level Monte Carlo generator CASCADE*, *Eur. Phys. J. C* **19** (2001) 351 [hep-ph/0012143] [INSPIRE].

[10] B.R. Webber, *A QCD Model for Jet Fragmentation Including Soft Gluon Interference*, *Nucl. Phys. B* **238** (1984) 492 [INSPIRE].

[11] M. Bengtsson, T. Sjöstrand and M. van Zijl, *Initial State Radiation Effects on W and Jet Production*, *Z. Phys. C* **32** (1986) 67 [INSPIRE].

[12] M. Bengtsson and T. Sjöstrand, *A Comparative Study of Coherent and Noncoherent Parton Shower Evolution*, *Nucl. Phys. B* **289** (1987) 810 [INSPIRE].

[13] G. Marchesini and B.R. Webber, *Monte Carlo Simulation of General Hard Processes with Coherent QCD Radiation*, *Nucl. Phys. B* **310** (1988) 461 [INSPIRE].

[14] B. Andersson, G. Gustafson and L. Lönnblad, *Gluon Splitting in the Color Dipole Cascades*, *Nucl. Phys. B* **339** (1990) 393 [INSPIRE].

[15] A.H. Mueller, *On the Multiplicity of Hadrons in QCD Jets*, *Phys. Lett. B* **104** (1981) 161 [INSPIRE].

[16] B.I. Ermolaev and V.S. Fadin, *Log-Log Asymptotic Form of Exclusive Cross-Sections in Quantum Chromodynamics*, *JETP Lett.* **33** (1981) 269 [INSPIRE].

[17] Y.L. Dokshitzer, V.S. Fadin and V.A. Khoze, *Coherent Effects in the Perturbative QCD Parton Jets*, *Phys. Lett. B* **115** (1982) 242 [INSPIRE].

[18] Y.L. Dokshitzer, V.S. Fadin and V.A. Khoze, *Double Logs of Perturbative QCD for Parton Jets and Soft Hadron Spectra*, *Z. Phys. C* **15** (1982) 325 [INSPIRE].

[19] Y.L. Dokshitzer, V.S. Fadin and V.A. Khoze, *On the Sensitivity of the Inclusive Distributions in Parton Jets to the Coherence Effects in QCD Gluon Cascades*, *Z. Phys. C* **18** (1983) 37 [INSPIRE].

[20] A. Bassetto, M. Ciafaloni, G. Marchesini and A.H. Mueller, *Jet Multiplicity and Soft Gluon Factorization*, *Nucl. Phys. B* **207** (1982) 189 [INSPIRE].

[21] B.R. Webber, *Monte Carlo Simulation of Hard Hadronic Processes*, *Ann. Rev. Nucl. Part. Sci.* **36** (1986) 253 [INSPIRE].

[22] M. Bengtsson and T. Sjöstrand, *Coherent Parton Showers Versus Matrix Elements: Implications of PETRA-PEP Data*, *Phys. Lett. B* **185** (1987) 435 [INSPIRE].

[23] J.C. Collins, *Spin Correlations in Monte Carlo Event Generators*, *Nucl. Phys. B* **304** (1988) 794 [INSPIRE].

[24] I.G. Knowles, *Angular Correlations in QCD*, *Nucl. Phys. B* **304** (1988) 767 [INSPIRE].

[25] I.G. Knowles, *Spin Correlations in Parton-Parton Scattering*, *Nucl. Phys. B* **310** (1988) 571 [INSPIRE].

[26] I.G. Knowles, *A Linear Algorithm for Calculating Spin Correlations in Hadronic Collisions*, *Comput. Phys. Commun.* **58** (1990) 271 [INSPIRE].

[27] S. Frixione and B.R. Webber, *Matching NLO QCD computations and parton shower simulations*, *JHEP* **06** (2002) 029 [hep-ph/0204244] [INSPIRE].

[28] P. Nason, *A new method for combining NLO QCD with shower Monte Carlo algorithms*, *JHEP* **11** (2004) 040 [hep-ph/0409146] [INSPIRE].

[29] S. Frixione, P. Nason and C. Oleari, *Matching NLO QCD computations with Parton Shower simulations: the POWHEG method*, *JHEP* **11** (2007) 070 [arXiv:0709.2092] [INSPIRE].

[30] S. Alioli, P. Nason, C. Oleari and E. Re, *A general framework for implementing NLO calculations in shower Monte Carlo programs: the POWHEG BOX*, *JHEP* **06** (2010) 043 [arXiv:1002.2581] [INSPIRE].

[31] S. Höche, F. Krauss, M. Schönherr and F. Siegert, *Automating the POWHEG method in Sherpa*, *JHEP* **04** (2011) 024 [arXiv:1008.5399] [INSPIRE].

[32] S. Hoeche, F. Krauss, M. Schönherr and F. Siegert, *A critical appraisal of NLO+PS matching methods*, *JHEP* **09** (2012) 049 [arXiv:1111.1220] [INSPIRE].

[33] J. Alwall et al., *The automated computation of tree-level and next-to-leading order differential cross sections, and their matching to parton shower simulations*, *JHEP* **07** (2014) 079 [arXiv:1405.0301] [INSPIRE].

JHEP10(2023)091

[34] S. Catani, F. Krauss, R. Kuhn and B.R. Webber, *QCD matrix elements + parton showers*, *JHEP* **11** (2001) 063 [hep-ph/0109231] [INSPIRE].

[35] L. Lönnblad, *Correcting the color dipole cascade model with fixed order matrix elements*, *JHEP* **05** (2002) 046 [hep-ph/0112284] [INSPIRE].

[36] F. Krauss, *Matrix elements and parton showers in hadronic interactions*, *JHEP* **08** (2002) 015 [hep-ph/0205283] [INSPIRE].

[37] J. Alwall et al., *Comparative study of various algorithms for the merging of parton showers and matrix elements in hadronic collisions*, *Eur. Phys. J. C* **53** (2008) 473 [arXiv:0706.2569] [INSPIRE].

[38] S. Hoeche, F. Krauss, S. Schumann and F. Siegert, *QCD matrix elements and truncated showers*, *JHEP* **05** (2009) 053 [arXiv:0903.1219] [INSPIRE].

[39] L. Lönnblad and S. Prestel, *Matching Tree-Level Matrix Elements with Interleaved Showers*, *JHEP* **03** (2012) 019 [arXiv:1109.4829] [INSPIRE].

[40] T. Gehrmann et al., *NLO QCD matrix elements + parton showers in $e^+e^- \to$ hadrons*, *JHEP* **01** (2013) 144 [arXiv:1207.5031] [INSPIRE].

[41] S. Hoeche, F. Krauss, M. Schönherr and F. Siegert, *QCD matrix elements + parton showers: The NLO case*, *JHEP* **04** (2013) 027 [arXiv:1207.5030] [INSPIRE].

[42] R. Frederix and S. Frixione, *Merging meets matching in MC@NLO*, *JHEP* **12** (2012) 061 [arXiv:1209.6215] [INSPIRE].

[43] L. Lönnblad and S. Prestel, *Merging Multi-leg NLO Matrix Elements with Parton Showers*, *JHEP* **03** (2013) 166 [arXiv:1211.7278] [INSPIRE].

[44] S. Plätzer, *Controlling inclusive cross sections in parton shower + matrix element merging*, *JHEP* **08** (2013) 114 [arXiv:1211.5467] [INSPIRE].

[45] Z. Nagy and D.E. Soper, *Matching parton showers to NLO computations*, *JHEP* **10** (2005) 024 [hep-ph/0503053] [INSPIRE].

[46] Z. Nagy and D.E. Soper, *A new parton shower algorithm: Shower evolution, matching at leading and next-to-leading order level*, in the proceedings of the *Ringberg Workshop on New Trends in HERA Physics 2005*, Ringberg Castle, Tegernsee, Germany, October 2–7, 2005, p. 101–123 [DOI:10.1142/9789812773524_0010] [hep-ph/0601021] [INSPIRE].

[47] S. Schumann and F. Krauss, *A parton shower algorithm based on Catani-Seymour dipole factorisation*, *JHEP* **03** (2008) 038 [arXiv:0709.1027] [INSPIRE].

[48] W.T. Giele, D.A. Kosower and P.Z. Skands, *A simple shower and matching algorithm*, *Phys. Rev. D* **78** (2008) 014026 [arXiv:0707.3652] [INSPIRE].

[49] S. Plätzer and S. Gieseke, *Coherent Parton Showers with Local Recoils*, *JHEP* **01** (2011) 024 [arXiv:0909.5593] [INSPIRE].

[50] S. Höche and S. Prestel, *The midpoint between dipole and parton showers*, *Eur. Phys. J. C* **75** (2015) 461 [arXiv:1506.05057] [INSPIRE].

[51] N. Fischer, S. Prestel, M. Ritzmann and P. Skands, *Vincia for Hadron Colliders*, *Eur. Phys. J. C* **76** (2016) 589 [arXiv:1605.06142] [INSPIRE].

[52] B. Cabouat and T. Sjöstrand, *Some Dipole Shower Studies*, *Eur. Phys. J. C* **78** (2018) 226 [arXiv:1710.00391] [INSPIRE].

JHEP10(2023)091

[53] M. Dasgupta et al., *Logarithmic accuracy of parton showers: a fixed-order study*, *JHEP* **09** (2018) 033 [*Erratum ibid.* **03** (2020) 083] [arXiv:1805.09327] [INSPIRE].

[54] M. Dasgupta et al., *Parton showers beyond leading logarithmic accuracy*, *Phys. Rev. Lett.* **125** (2020) 052002 [arXiv:2002.11114] [INSPIRE].

[55] Z. Nagy and D.E. Soper, *Parton shower evolution with subleading color*, *JHEP* **06** (2012) 044 [arXiv:1202.4496] [INSPIRE].

[56] S. Plätzer and M. Sjödahl, *Subleading N_c improved Parton Showers*, *JHEP* **07** (2012) 042 [arXiv:1201.0260] [INSPIRE].

[57] Z. Nagy and D.E. Soper, *A parton shower based on factorization of the quantum density matrix*, *JHEP* **06** (2014) 097 [arXiv:1401.6364] [INSPIRE].

[58] Z. Nagy and D.E. Soper, *Effects of subleading color in a parton shower*, *JHEP* **07** (2015) 119 [arXiv:1501.00778] [INSPIRE].

[59] S. Plätzer, M. Sjödahl and J. Thorén, *Color matrix element corrections for parton showers*, *JHEP* **11** (2018) 009 [arXiv:1808.00332] [INSPIRE].

[60] J. Isaacson and S. Prestel, *Stochastically sampling color configurations*, *Phys. Rev. D* **99** (2019) 014021 [arXiv:1806.10102] [INSPIRE].

[61] Z. Nagy and D.E. Soper, *Exponentiating virtual imaginary contributions in a parton shower*, *Phys. Rev. D* **100** (2019) 074005 [arXiv:1908.11420] [INSPIRE].

[62] Z. Nagy and D.E. Soper, *Parton showers with more exact color evolution*, *Phys. Rev. D* **99** (2019) 054009 [arXiv:1902.02105] [INSPIRE].

[63] J.R. Forshaw, J. Holguin and S. Plätzer, *Parton branching at amplitude level*, *JHEP* **08** (2019) 145 [arXiv:1905.08686] [INSPIRE].

[64] S. Höche and D. Reichelt, *Numerical resummation at subleading color in the strongly ordered soft gluon limit*, *Phys. Rev. D* **104** (2021) 034006 [arXiv:2001.11492] [INSPIRE].

[65] M. De Angelis, J.R. Forshaw and S. Plätzer, *Resummation and Simulation of Soft Gluon Effects beyond Leading Color*, *Phys. Rev. Lett.* **126** (2021) 112001 [arXiv:2007.09648] [INSPIRE].

[66] J. Holguin, J.R. Forshaw and S. Plätzer, *Improvements on dipole shower colour*, *Eur. Phys. J. C* **81** (2021) 364 [arXiv:2011.15087] [INSPIRE].

[67] K. Hamilton et al., *Colour and logarithmic accuracy in final-state parton showers*, *JHEP* **03** (2021) 041 [arXiv:2011.10054] [INSPIRE].

[68] S. Höche, D. Reichelt and F. Siegert, *Momentum conservation and unitarity in parton showers and NLL resummation*, *JHEP* **01** (2018) 118 [arXiv:1711.03497] [INSPIRE].

[69] G. Bewick, S. Ferrario Ravasio, P. Richardson and M.H. Seymour, *Logarithmic accuracy of angular-ordered parton showers*, *JHEP* **04** (2020) 019 [arXiv:1904.11866] [INSPIRE].

[70] J.R. Forshaw, J. Holguin and S. Plätzer, *Building a consistent parton shower*, *JHEP* **09** (2020) 014 [arXiv:2003.06400] [INSPIRE].

[71] M. van Beekveld et al., *PanScales parton showers for hadron collisions: formulation and fixed-order studies*, *JHEP* **11** (2022) 019 [arXiv:2205.02237] [INSPIRE].

[72] S. Catani and M.H. Seymour, *A general algorithm for calculating jet cross-sections in NLO QCD*, *Nucl. Phys. B* **485** (1997) 291 [hep-ph/9605323] [INSPIRE].

JHEP10(2023)091

[73] S. Höche and S. Prestel, *Triple collinear emissions in parton showers*, *Phys. Rev. D* **96** (2017) 074017 [arXiv:1705.00742] [INSPIRE].

[74] F. Dulat, S. Höche and S. Prestel, *Leading-Color Fully Differential Two-Loop Soft Corrections to QCD Dipole Showers*, *Phys. Rev. D* **98** (2018) 074013 [arXiv:1805.03757] [INSPIRE].

[75] T. Gleisberg et al., *SHERPA 1. alpha: A proof of concept version*, *JHEP* **02** (2004) 056 [hep-ph/0311263] [INSPIRE].

[76] T. Gleisberg et al., *Event generation with SHERPA 1.1*, *JHEP* **02** (2009) 007 [arXiv:0811.4622] [INSPIRE].

[77] SHERPA collaboration, *Event Generation with Sherpa 2.2*, *SciPost Phys.* **7** (2019) 034 [arXiv:1905.09127] [INSPIRE].

[78] K. Hamilton et al., *Soft spin correlations in final-state parton showers*, *JHEP* **03** (2022) 193 [arXiv:2111.01161] [INSPIRE].

[79] A. Bassetto, M. Ciafaloni and G. Marchesini, *Jet Structure and Infrared Sensitive Quantities in Perturbative QCD*, *Phys. Rept.* **100** (1983) 201 [INSPIRE].

[80] R.K. Ellis, W.J. Stirling and B.R. Webber, *QCD and collider physics*, Cambridge University Press (2011) [DOI:10.1017/CBO9780511628788] [INSPIRE].

[81] V.V. Sudakov, *Vertex parts at very high-energies in quantum electrodynamics*, *Sov. Phys. JETP* **3** (1956) 65 [INSPIRE].

[82] T. Sjöstrand, S. Mrenna and P.Z. Skands, *PYTHIA 6.4 Physics and Manual*, *JHEP* **05** (2006) 026 [hep-ph/0603175] [INSPIRE].

[83] S. Catani, L. Trentadue, G. Turnock and B.R. Webber, *Resummation of large logarithms in e^+e^- event shape distributions*, *Nucl. Phys. B* **407** (1993) 3 [INSPIRE].

[84] A. Banfi, G.P. Salam and G. Zanderighi, *Principles of general final-state resummation and automated implementation*, *JHEP* **03** (2005) 073 [hep-ph/0407286] [INSPIRE].

[85] M. Schönherr and F. Krauss, *Soft Photon Radiation in Particle Decays in SHERPA*, *JHEP* **12** (2008) 018 [arXiv:0810.5071] [INSPIRE].

[86] Z. Nagy and D.E. Soper, *Summations by parton showers of large logarithms in electron-positron annihilation*, arXiv:2011.04777 [INSPIRE].

[87] E. Farhi, *A QCD Test for Jets*, *Phys. Rev. Lett.* **39** (1977) 1587 [INSPIRE].

[88] S. Catani, G. Turnock and B.R. Webber, *Jet broadening measures in e^+e^- annihilation*, *Phys. Lett. B* **295** (1992) 269 [INSPIRE].

[89] JADE and OPAL collaborations, *QCD analyses and determinations of α_s in e^+e^- annihilation at energies between 35-GeV and 189-GeV*, *Eur. Phys. J. C* **17** (2000) 19 [hep-ex/0001055] [INSPIRE].

[90] ALEPH collaboration, *Studies of QCD at e^+e^- centre-of-mass energies between 91-GeV and 209-GeV*, *Eur. Phys. J. C* **35** (2004) 457 [INSPIRE].

[91] S. Catani, B.R. Webber and G. Marchesini, *QCD coherent branching and semiinclusive processes at large x*, *Nucl. Phys. B* **349** (1991) 635 [INSPIRE].

[92] G.S. Chahal and F. Krauss, *Cluster Hadronisation in Sherpa*, *SciPost Phys.* **13** (2022) 019 [arXiv:2203.11385] [INSPIRE].

[93] A. Buckley et al., *Rivet user manual*, *Comput. Phys. Commun.* **184** (2013) 2803 [arXiv:1003.0694] [INSPIRE].

JHEP10(2023)091

[94] G. Gustafson, *Multiplicity distributions in QCD cascades*, *Nucl. Phys. B* **392** (1993) 251 [INSPIRE].

[95] L. Gellersen, S. Höche and S. Prestel, *Disentangling soft and collinear effects in QCD parton showers*, *Phys. Rev. D* **105** (2022) 114012 [arXiv:2110.05964] [INSPIRE].

[96] S. Höche, S. Liebschner and F. Siegert, *Resonance-Aware Subtraction in the Dipole Method*, *Eur. Phys. J. C* **79** (2019) 728 [arXiv:1807.04348] [INSPIRE].

[97] S. Liebschner, *On the Treatment of Colour-Charged Resonances in Precision Calculations of Monte Carlo Generators*, http://cds.cern.ch/record/2735199.

[98] G. Curci, W. Furmanski and R. Petronzio, *Evolution of Parton Densities Beyond Leading Order: The Nonsinglet Case*, *Nucl. Phys. B* **175** (1980) 27 [INSPIRE].

JHEP10(2023)091